INTERNATIONAL REVIEWS IN PHYSICAL CHEMISTRY
2020, VOL. 39, NO. 4, 569–623
https://doi.org/10.1080/0144235X.2020.1826708

Taylor & Francis
Taylor & Francis Group

Fundamentals of ion mobility in the free molecular regime. Interlacing the past, present and future of ion mobility calculations

Carlos Larriba-Andaluz [a] and James S. Prell[b]

[a]Department of Mechanical Engineering, Indiana University-Purdue University Indianapolis, Indianapolis, IN, USA; [b]Department of Chemistry and Biochemistry, University of Oregon, Eugene, OR, USA

ABSTRACT

While existing ion mobility calculators are capable of feats as impressive as calculating collision cross sections (CCS) within a few per cent and within a very reasonable time, the simplifications assumed in their estimations precludes them from being more precise, potentially overreaching with respect to the interpretation of existing calculations. With ion mobility instrumentation progressively reaching resolutions of several hundreds to thousands (accuracy in the range of $\sim$0.1%), a more accurate theoretical description of gas-phase ion mobility becomes necessary to correctly interpret experimental state-of-the-art separations. This manuscript entails an effort to consolidate the most relevant theoretical work pertaining to ion mobility within the 'free molecular' regime, describing in detail the rationale for approximations up to the two-temperature theory, using both a momentum transfer approach as well as the solution to the moments of the Boltzmann equation for the ion. With knowledge of the existing deficiencies in the numerical methods, the manuscript provides a series of necessary additions in order to better simulate some of the separations observed experimentally due to second-order effects, namely, high field effects, dipole alignment, angular velocities and moments of inertia, potential interactions and inelastic collisions among others.

ARTICLE HISTORY
Received 9 April 2020
Accepted 17 September 2020

KEYWORDS
Ion; mobility; drift; two-temperature; kinetic theory; free molecular

Contents

CONTACT Carlos Larriba-Andaluz clarriba@iupui.edu Department of Mechanical Engineering, Indiana University-Purdue University Indianapolis, 723 W Michigan St. SL260, Indianapolis, IN 46202

This article was originally published with errors, which have now been corrected in the online version and in print. Please see Correction https://doi.org/10.1080/0144235X.2020.1860380

1. Introduction

In its most formal definition, Ion/Electrical Mobility (IM) is a transport property that describes the ability of an ion, i.e. charged molecule/cluster/particle, to traverse a gas medium by means of the energy provided by an external electric field. As the ion travels, the way it interacts with the gas medium varies substantially depending on the flow regime and scale. When referring to IM in the 'free molecular' regime, it is also assumed that the ion/charged entity does not 'significantly' perturb the gas, i.e. when the characteristic size of the ion is much smaller than the mean free path of the gas. Under free molecular flow, ion mobility is necessarily a function of the gas thermodynamic properties (pressure, temperature, mass, size, internal degrees of freedom), those of the ion, any existing interaction potentials (e.g. Lennard-Jones-like, ion-dipole, or ion-quadrupole interactions), and the energy exchange involved in the process. As is normally the case for other transport properties, the value referenced as IM is an average value for a large enough ensemble of ions over many collisions rather than a value at any given instant. As the inertial force provided by the external electric field is balanced by the net collisional drag – a balance that is achieved extremely quickly – a drift velocity is reached that depends on the mobility through [1]:

$$\vec{v}_d = \overline{\overline{K}} \cdot \vec{E}, \tag{1}$$

where $\vec{v}_d$ is the drift velocity, $\overline{\overline{K}}$ is the mobility tensor and $\vec{E}$ is the electric field. $\overline{\overline{K}}$, in principle, may be assumed to be a second-order tensor since the drift velocity does not necessarily have to be in the direction of the field. However, under most circumstances of interest for small ions, i.e. when all orientations are equally probable, electric field and total average displacement per unit time may be considered to be in the same direction, and thus ion mobility can be described by a single value, K, instead of a tensor, i.e. $\langle v_d \rangle = \langle K \rangle \cdot E$ [2].

The most detailed calculations concerning Ion Mobility are performed by studying the collision energy exchange between ion and gas molecules. In order to accurately calculate this collisional interaction, it is necessary to know the velocity distribution function of both ions and gas. Under the free molecular regime, the buffer gas distribution function may be assumed, while the ion's distribution may only be obtained either through an informed guess or by solving the Boltzmann equation (an integrodifferential equation which contains a convoluted collisional term) [3]. To make the Boltzmann equation more manageable, a series of reasonable simplifications are typically used. The most significant of such simplifications, aside from the gas being perceived as having a well-behaved Maxwell–Boltzmann distribution, is that the number density of ions is much smaller than that of the gas molecules, i.e. ions are so far apart from each other that they do not interact. This reduces the complexity of the collision term, which then has only a binary interaction between gas molecule and ion and is directly related to the differential cross section and

relative scattering of the pair. This modification alone is still commonly insufficient, and further simplifications, such as fitted interaction potentials or elasticity of collisions, are required to provide suitable estimates and approximations to the integral.

Even under such a plethora of simplifications, only a few different theoretical approaches to solving the Boltzmann equation have been explored in detail, and many times the only analytical solutions that exist are left as quadratures of particular moments of the distribution, i.e. the average velocity, or the kinetic energy of the ion, but not the distribution itself [4]. Solving only the first few moments may not seem ideal at first, but it turns out that, most experiments will provide the user with only a particular property of the ion that is related to one of the moments of the distribution (the average velocity for example would yield the mobility) and therefore there is no need to know the distribution function in full detail. However, the resulting quadratures generally depend on the geometry of the ion, the interaction potential, the strength of the field, and the scattering of the gas molecules on the surface, and hence their calculation must be addressed numerically, except perhaps for particularly simple cases [5]. Despite the intricacy behind the calculations and the simplifications noted, numerically obtained solutions yield seemingly accurate mobility values when compared to experimental results, notably when reasonable procedures are in place, with some of the more computationally expensive methods reaching accuracies of a few per cent($< \sim 4\%$); mainly under small to vanishing fields and parametrised interaction potentials [6].

A problem that arises when comparing numerical and experimental results is that the accuracy of experimental mobilities is difficult to define as it depends on the equipment and method used, as well as on the type of molecule being analysed, e.g. the accuracy of the same system may be different when dealing with flexible versus rigid molecules [7–10]. Nonetheless, with proper calibrations, it has been shown that experimental calculations can be normalised to a degree even across different systems and laboratories [11,12]. Within a single run, and based on shifts with respect to a given calibrant (which may have its own uncertainties), recent experimental advances, however, demonstrate the ability of systems to achieve accuracies of less than 1% [13–19], or even less than 0.1% (resolutions in excess of 1000) [20], transcending the accuracy of our state-of-the-art theoretically derived approximations. Experimental achievements of this magnitude should not be overlooked, as they open up the possibility of separation of ions with nearly identical structures, such as stereoisomers, regioisomers, isotopologues, or even isotopomers [21–26], and where separation of ions may only be possible through second- or higher-order effects (difference in potential interactions, high external fields, dipole moments, field alignment, charge locations, difference in moments of inertia, ...). The key realisation here is that, with accuracies of a few per cent, the existing theoretical framework may often be insufficient to provide a full explanation for IM separation of species observed in state-of-the-art and futuristic experiments.

This review addresses three eras of IM theory: (past) an accurate description of the existing background knowledge on IM, (present) to establish the current state of the field from a theoretical-numerical perspective, and (future) to establish the drawbacks of the existing theory, how to overcome the existing limitations, and propose further advancement in ion mobility calculations.

The theoretical background (past) includes a critical insight into collision cross section calculations and includes several higher-order approximations to the Mason-Schamp

equation, including and up to the two-temperature theory, so as to provide a more detailed account of the simplifications leading to the equation. This section is supplemented with three appendices that provide a comprehensive description of the theoretical approach. The numerical description (present) accounts for the most relevant numerical approaches to the calculation of ion mobility and collision integrals and weighs in on possible extensions to the calculations. The last section is devoted to reinforcing the validity of the numerical calculations and establishing possible drawbacks to the existing theory and numerical approaches. In particular, the relaxation of the equal orientation probability assumption is discussed in detail to allow effects such as rotation, moments of inertia, dipole moments and general alignments to be considered. In all, there is a need for a well-founded theory to interpret and to understand the high separation achieved by novel systems.

2. Theoretical background

The purpose of this section is to provide the readers with ample critical insight to understand the accuracy of the most common expressions used to calculate mobility of ions/charged nanoparticles in the free molecular regime. For that, it seems helpful to make a distinction between two contemporary fields pursuing the study of ion/electrical mobility: aerosol science and analytical/physical chemistry. The reason for the bifurcation into two is that seemingly related interests in mobility calculations were somewhat isolated from each other until the 1990–2000s with the work of Fernandez de la Mora and coworkers successfully studying ions with tools mostly reserved to aerosol nanoparticles [27–31]. The separation between these two fields made sense at the beginning, as aerosol particles of interest were in general very large and mostly out of the free molecular regime. As instruments became more precise and nanoparticles (i.e. within the free molecular regime) started to be ubiquitously studied, both trends started converging with shared interests. And although existing theories seemed to initially offer some disparate results, it has become apparent that their results are indeed consistent if the premises are interpreted correctly. From that perspective, this section will mostly focus on kinetic theory and ion transport, traditionally used to understand smaller ions, with only brief inclusions from aerosol physics. Given the multiple theoretical classifications involved in the study of Ion Mobility, a summary of the most notable differences is provided in Table 1.

Before introducing the results of kinetic theory, it is conventional to bring up two other theories which share qualitative results with kinetic theory: free-flight and momentum transfer theories. Free-flight (sometimes referred to as free path) theory is based on the notion of a mean time or distance travelled between collisions. Its largest exponent is Wannier who produced some results that agree remarkably well with the more accurate kinetic theory results [32–34]. In particular, Wannier's energy formula was initially derived using free-flight, and its repercussions will be discussed later on. By contrast, momentum transfer theory is based on solving the collisional integral using an expansion in terms of pure momentum exchange arguments (as shown in Appendix A). This theory dates back as far as Maxwell [35], with Langevin being the first to provide a quantitative low-field mobility theory [36]. Langevin's results were later used by many authors, including Lenard, Cunningham and Epstein [37–39]. Epstein, upon request from Millikan [40], provided a result for ion mobility using laws of reflection and an 'accommodation coefficient' that has been extensively used in the aerosol field.

Table 1. Classification of theoretical approaches to ion mobility.

By Theoretical Model	**Momentum Transfer Theory**. The idea behind the momentum transfer theory is to calculate the momentum gained by the ion due to the presence of the field. This is done by equating this momentum to the drag force caused by the gas molecule impingement imbalance. Explained in Appendix A.
	Mean Free Path Theory. The mean free path theory is a simplistic model based on the notion of a mean time or distance travelled between collisions. Its largest exponent is Wannier, who produced some results that agree remarkably well with the more accurate kinetic theory results.
	Kinetic Theory. Based on solving the first few moments of the Boltzmann equation or a related equation (See the Wang-Chang-Uhlenbeck-De Boer (WUB) equation). For a derivation of the one-temperature theory and two-temperature kinetic theories, see appendices B and C respectively.
By Field Strength	**Vanishing Fields**. This is the Chapman-Enskog linearised solution. Its maximum exponent is Equation (2), which is only valid for $E/n \sim 0$.
	Weak Fields. Kihara's extension of the Chapman-Enskog solution by including higher-order approximations. It is equivalent to the one-temperature kinetic theory. It is valid only for weak fields due to the poor convergence of the approximation terms (see Figure 1(a)). Mason and Schamp modified how higher-order approximations are calculated, and their result is shown in Equations (7)–(8) and in Appendix B.
	Full E/n Range. There are many theories that cover the full E/n range. Among such theories, one can name the two-temperature theory, three-temperature theory, and WUB equation. The first approximations of the two-temperature theory appear in Equations (12)–(13) and in Appendix C.
By Temperature of the Ion	**One-Temperature Theory**. Equivalent to Kihara's theory. The zeroth order ion distribution function is chosen to be an equilibrium Maxwellian at the gas temperature. Only valid for weak fields. See Equations (7)–(8) and Appendix B.
	Two-Temperature Theory. The temperature of the zeroth order ion distribution is assumed to be an adjustable parameter that may be different from the gas temperature. Most of the time, it is assumed to be equivalent to the ion temperature calculated through the mean ion energy and Wannier's relation Equations (9). See Equations (12)–(13) and Appendix C.
	Three-Temperature Theory. Similar to the two-temperature theory but it suggests that ion temperature is different in longitudinal and transverse directions. Mainly useful for heavy ions where the two-temperature theory fails. Not studied in this work.
By Mass Ratio	**Lorentz Model**. Mass of the ion is much smaller than the mass of the gas ($m >> M$), e.g. electrons. The analytical solution to ion mobility is known exactly for this case, and hence it is commonly used as a reference to analyse other general expressions.
	Rayleigh Model. Mass of the ion is much larger than the mass of the gas ($M >> m$), e.g. aerosols. For cases of low fields, the ion distribution for the Rayleigh model is assumed as shown in Appendix A.
By Type of Collision	**Elastic Collisions**. The collisions between gas and ions are assumed to be perfectly elastic. Only strictly valid for monoatomic entities (gas and ions).
	Inelastic Collisions. There is an energy transfer between the different degrees of freedom (including ro-vibrational) upon a gas-ion collision. For aerosols, Langevin, Lenard and Epstein assume the effect of inelasticity through an accommodation coefficient (see Equations 15a-b). For kinetic theory, inelastic collisions may be accounted for through the WUB equation, which accounts for interactions of polyatomic ions and polyatomic gases. The WUB equation is not studied in this work.

The use of kinetic theory to calculate ion mobility comes from its close relation with diffusion through Einstein's relation. Although progress in this area started with Maxwell and Boltzmann [41,42], the rigorous derivations of transport properties came at the hands of Chapman & Enskog [43], who were the first to provide suitable expressions for ion mobility under vanishingly small electric fields. Their result, as recollected in the treatise by Chapman and Cowling was left as a quadrature due to the difficulty arising from the potential interaction relation between gas and ion, except perhaps for simplified, unrealistic potentials. Hasse was pioneer in using a more reasonable 4-∞ potential that accounted for the polarisability of the gas and the hard sphere repulsion. This was later modified to

a 4–8 potential to account for a softer repulsion [44,45]. Experimental results, however, suggested that the repulsion was somewhere in between the two repulsion exponents and that dispersion forces and even charge-quadrupole terms could be significant [46–48]. A breakthrough was accomplished by Taro Kihara, who was the first to extend the Chapman-Enskog theory to non-vanishing fields by providing approximations to the solution of the velocity moment of the Boltzmann equation using modified Burnett functions [49]. Kihara's approximation to the mobility for non-vanishing fields was explored by Mason and Schamp using numerical predictions to investigate an attractive-repulsive $4-n$ law, with n ranging from 8 to infinity. This led to the more well-known version of Kihara's first approximation for zero field, the Mason-Schamp's equation [50]:

$$\langle K\rangle_I = \frac{3}{16}\frac{ze}{n}\left(\frac{2\pi}{\mu kT}\right)^{\frac{1}{2}}\frac{1}{\bar{\Omega}_T(1,1)}. \tag{2}$$

Equation (2) represents the mobility of an ion of mass M and charge ze in a bath gas of mass m and number density n. Here k is the Boltzmann constant, μ is the reduced mass, T is the temperature of the gas and ion (assumed to be the same), and $\bar{\Omega}_T(1,1)$ is the orientationally averaged collision cross section (CCS) integral, where the subscript T refers to the fact that the CCS integral is calculated at temperature T. The orientationally averaged CCS in this equation is given by [51]:

$$\begin{aligned}\bar{\Omega}_T(1,1) = \frac{1}{8\pi^2}\int_0^{2\pi} d\theta \int_0^{\pi} \sin\phi d\phi \int_0^{2\pi} d\gamma \frac{\pi}{8}\left(\frac{\mu}{kT}\right)^3 \int_0^{\infty} g^5 e^{-\frac{\mu g^2}{2kT}} dg \\ \times \int_0^{\infty} 2b(1-\cos\chi(\theta,\phi,\gamma,g,b))db.\end{aligned} \tag{3}$$

In this equation, θ, ϕ, and γ are the 3 orientation angles of the ion, g is the relative velocity, b is the impact parameter, μ is the reduced mass, and χ is the deflection angle. χ depends on the ion-gas interaction potentials, the relative velocity of the ion-gas, the impact parameter, and the orientation of the ion as [3]:

$$\chi(\phi,\theta,\gamma,g,b) = \pi - 2b\int_{r_m}^{\infty} \frac{dr}{r^2\sqrt{1-\frac{b^2}{r^2}-\frac{\Phi(r)}{\frac{\mu g^2}{2}}}}. \tag{4}$$

r is the ion-gas molecule distance, r_m is the distance of closest approach and $\Phi(r)$ is the ion-gas interaction potential. To reach the expression in Equation (4) (see Appendix A), the interaction potential is assumed to be caused by a central force. Even when the interaction potential $\Phi(r)$ is known under such simplifications, Equation (4) cannot be calculated analytically except for the simplest cases, thus requiring the deflection angle χ to be calculated numerically.

It should be emphasised that, in Equations (2)–(4), a single temperature is used to describe both the ion and gas. However, it is quite possible physically that the ion has a different temperature from the gas, in particular when a high field is present and acting on the ion. For this reason, the above theory is called the one-temperature theory, in contrast to the two-temperature theory, in which the ion and gas have different temperatures, or to the three-temperature theory, in which separate longitudinal and transverse temperatures of the ion are also considered.

Equation (2) can be obtained in different ways, two of which are presented in the Appendix. The first is through a momentum transfer approach (see Appendix A), and the second is through kinetic theory and the one-temperature theory (see Appendix B). The momentum transfer theory calculates the mobility by simple arguments of momentum loss or drag force, F_D, required to reach equilibrium:

$$qE_i = F_{Di} = B_{ij}v_{dj} \tag{5a-b}$$

where B_{ij} is the drag tensor and $q\langle B_{ij}\rangle^{-1} = \langle K\rangle$. The procedure to calculate $\langle B_{ij}\rangle$ starts from the presumption that the velocity distribution of ions can be represented by a Maxwell distribution that is skewed by the drift velocity (see Appendix A for more details) [43]:

$$F_{M\gg m}(z_i) = \left(\frac{M}{2\pi kT}\right)^{3/2} e^{-\frac{M(z_i - v_{di})^2}{2kT}}, \tag{6}$$

where z_i is the (vector) velocity of the ion. This assumption of the ion velocity distribution and the use of a single temperature for gas and ion is most valid for large ions and nanoparticles ($M \gg m$) in vanishing fields in what has been called the Rayleigh model in honour of the work done by Lord Rayleigh for heavy particles in a light gas [52]. Mobility results using a similar concept were already calculated by Epstein back in 1924 trying to match results from Millikan's oil drop experiments. In short, the imposed ion velocity distribution in Equation (6) is used to calculate the average number of collisions per unit time, and with it the total average momentum, and hence the drag force. If a non-spherical ion is assumed fixed in space during collisions, the resulting drift velocity may not be in the direction of the field, making the calculation tensorial and requiring at least 3 perpendicular directions to obtain a symmetric matrix (B_{ij}) that needs to be averaged. The averaging of the tensor product on the right-hand side of Equation (5b) has been the subject of a lot of controversy, although some of it has been recently resolved [53]. It suffices to say here that the general averaged result from Happel and Brenner used in aerosol science to calculate mobilities does not match Equation (2) and should not be used to calculate ion mobility as it calculates the average length of the path travelled in the direction of the velocity rather than just its projection in the direction of the field. To avoid this difficulty, Appendix A shows a non-tensorial version of the calculation of the drag force that matches Mason and Schamp's result.

While eye-opening, the results from Appendix A require one to make assumptions about the ions' velocity distribution. This assumption might lead to wrong conclusions if the incorrect ion distribution is chosen. In fact, as it is shown in Appendix B, the ion distribution provided in Equation (6) is only valid for vanishing fields and large ions, and, without proper corrections (e.g. using the proper ion temperature), would fail to give the correct value of ion mobility under other circumstances. Without proper knowledge of the ion distribution, one must resort to the Boltzmann equation and its moments again. Kihara's method, with slight modifications from Mason and Schamp, may be then used to obtain higher-order corrections to Equation (2) for non-vanishing fields. Appendix B follows a detailed account on how to obtain these higher-order approximations under the assumption of a one-temperature theory. For example, a third-order approximation may

be given by [50]:

$$\langle K\rangle_{III} = \langle K\rangle_I \left[\alpha_0 + \alpha_1\left(\frac{\mathcal{E}}{a_{00}(1)}\right)^2 + \alpha_2\left(\frac{\mathcal{E}}{a_{00}(1)}\right)^4 + \cdots\right], \tag{7}$$

with $\mathcal{E} = (eE/Mn)(M/2kT)^{1/2}$ being the modified electric field strength. The α_i terms are functions of the $a_{rs}(l)$ terms which themselves depend on collision integrals. For example, the term α_0 is given by [50]:

$$\alpha_0 = 1 + \frac{a_{01}(1)}{a_{00}(1)}\frac{a_{10}(1)}{a_{11}(1)} + \frac{a_{02}(1)}{a_{00}(1)}\frac{a_{20}(1)}{a_{22}(1)} + \cdots \tag{8}$$

Here, the $a_{rs}(l)$ are the matrix coefficients used to evaluate the Lorentzian operator using Burnett's basis functions. The determination of the first 3 α_i and some of the $a_{rs}(l)$ coefficients is also given in Appendix B together with a table for the rest of the coefficients needed in Equation (7).

There are a couple of important observations regarding Equation (7). The first one is that higher approximations have a dependence on even powers of the field only. A second one (which is addressed in Appendices B and C) is that the $a_{rs}(l)$ terms depend on ratios of ion and gas masses (M and m). This forces the description of Equation (7) to be done in terms not only of different approximations but also of different m/M ratios. A third observation is that a correction to mobility still exists even for vanishing fields ($\mathcal{E} \sim 0$) due to the extra terms in α_0. These terms provide a very small correction (up to a few per cent for electrons but much lower for larger ions) that increases with the ratio m/M and is most important for the Lorentz model ($m \gg M$) [54]. The second is that, while it might appear that expression (7) is general for any field, it turns out that its convergence is very poor due to the unbound nature of $(\mathcal{E}/(a_{00}(1)))^n$, which increases as the field increases, requiring higher and higher approximations for higher fields. Since the α_i terms become increasingly more difficult to calculate, it precludes any advantage of using Equation (7) for anything but weak fields.

This poor convergence is shown in Figure 1(a) for the case $m \gg M$ (Lorentz model, i.e. for electrons) as it is the only case for which an analytical solution is exactly known. In the figure, a dimensionless drift velocity v_d^* is shown as a function of a dimensionless ε^* for rigid spheres:

$$\varepsilon^* = \left(\frac{3\pi^{1/2}}{16kT}\right)\left(\frac{m+M}{M}\right)^{1/2}\left(\frac{zeE}{n\pi d^2}\right)$$

$$v_d^* = \left(\frac{m}{2kT}\right)^{1/2} v_d$$

with d the diameter of the sphere of influence (radius of ion plus radius of gas). Neither the 2nd nor the 3rd approximation performs well as the field increases. Shown in the figure is another third-order approximation used by Kihara, which differs slightly from the former in the way it is derived [49,55]. In order to compare results for other mass ratios for which no exact solution is known, one would have to compare different degrees of approximation to estimate the accuracy. Given the poor convergence of the one-temperature

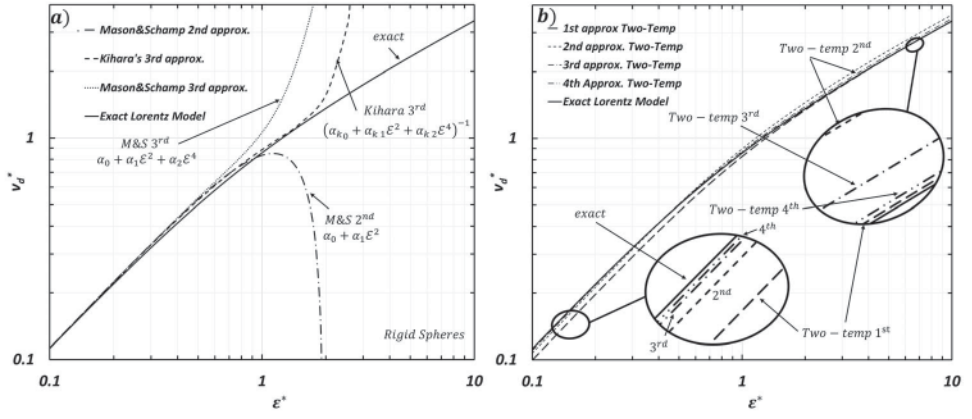

Figure 1. Comparison of results from different ion mobility models using dimensionless parameters. The dimensionless drift velocity, v_d^*, is shown as a function of the dimensionless electric field to gas concentration ratio, ε^*, for rigid spheres for the case $m/M \gg 1$ (Lorentz model), which is the only case for which the exact solution is known (solid line). The exact model is compared to (a) one-temperature theory including the second (Mason & Schamp) and third approximations (Mason & Schamp and Kihara) and (b) for the two-temperature theory including the 1st through 4th approximations (Mason & Viehland).

theory at higher fields, this comparison will be skipped for now and attempted for the two-temperature theory below.

A major factor leading to the divergence of these approximation from the exact Lorentz model at high field strengths is that these approximations assume a single temperature describing both the ion and the gas. Appendix B also calculates the ion's kinetic energy, $\frac{1}{2}M\langle z^2\rangle_I$, to a first approximation, which yields:

$$\frac{1}{2}M\langle z^2\rangle_I = \frac{3}{2}kT + \frac{1}{2}M\langle v_d\rangle_I^2 + \frac{1}{2}m\langle v_d\rangle_I^2, \tag{9}$$

where $\langle v_d\rangle_I = \langle K\rangle_I E$ is the first approximation to the drift velocity. The result of Equation (9) was produced for the first time by Wannier in the free-flight theory and seems to hold well under all scenarios studied here. The first term on the right-hand side corresponds to the thermal energy of the ion ($\frac{3}{2}kT$) in a bath gas at temperature T, the second term corresponds to the added kinetic energy of the ion due to the presence of the field ($\frac{1}{2}M\langle v_d\rangle_I^2$), while the last term corresponds to the increased energy due to gas-ion collisions ($\frac{1}{2}m\langle v_d\rangle_I^2$). Under most experimental scenarios with $M > m$, the two last terms are negligible as v_d^2 is very small, but care should be taken when they are not, i.e. when high fields are present or ions have $M \sim m$.

Given the result of Equation (9), a possible improvement over the one-temperature approximation is to allow for the gas and ion to have different temperatures [56,57]. By assigning a temperature T_b to the ion different from the gas temperature T, one can try to overcome the problems associated with the one-temperature theory. Intuitively, as the ion's drift velocity increases, its temperature will deviate from the gas temperature due to the increasing overall energy of the ion. A natural choice for ion temperature T_b emanates from Equation (9) so that $\frac{3}{2}kT_b = \frac{1}{2}M\langle z^2\rangle_I$. The incorporation of the ion temperature leads to the two-temperature theory which provides much better convergence than Equation (7)

for any field, even when using its first approximation [57]:

$$\langle K_{2T}\rangle_I = \frac{3}{16}\frac{ze}{n}\left(\frac{2\pi}{\mu k T_{eff}}\right)^{\frac{1}{2}}\frac{1}{\bar{\Omega}^*_{T_{eff}}(1,1)}, \tag{10}$$

which resembles Equation (2) but where T has been changed for the effective temperature T_{eff}:

$$\frac{3}{2}kT_{eff} = \frac{3}{2}kT + \frac{1}{2}m\langle v_d\rangle_I^2 \tag{11}$$

In this equation, $\bar{\Omega}^*_{T_{eff}}(1,1)$ is calculated by Equation (3) using T_{eff} instead of T. When compared to T_b, the effective temperature is the part of the temperature that directly affects the momentum transfer, leaving out the energy pertaining to the field, $\frac{1}{2}M\langle v_d\rangle_I^2$. Appendix C provides a careful derivation of Equation (10) as well as of the second approximation as provided by Viehland and Mason [57]:

$$\langle K_{2T}\rangle_{II} = \frac{3}{16}\frac{ze}{n}\left(\frac{2\pi}{\mu k T_{eff}}\right)^{\frac{1}{2}}\frac{1+\alpha^*}{\bar{\Omega}^*_{T_{eff}}(1,1)}, \tag{12}$$

with a higher-order correction to the effective temperature as well:

$$\frac{3}{2}kT_{eff} = \frac{3}{2}kT + \frac{1}{2}m\langle v_d\rangle_I^2(1+\beta^*). \tag{13}$$

Equation (12) together with Equation (13) encompasses some useful theoretical results without the need of overcomplicating the picture for mobility. Here α^* and β^* are higher-order corrections (with dependencies on even powers of the field as given in Appendix C), and where the * represents that their calculation involves the use of T_{eff} instead of T. Due to the loss of symmetry of the Lorentzian operator (see Appendix C), α^* differs from the α_i values in Equation (7). The introduction of T_{eff} however gets rid of the convergence problem of the one-temperature theory. In fact, Equations (10) and (12) have been shown to be within less than 10% of the exact theoretical result for any field for the Lorentz model ($m \gg M$), and Equation (12) provides a minor improvement over Equation (10) [56]. The results are shown in Figure 1(b) using the first four approximations as well as the exact value for the Lorentz model [55,56] in the same dimensionless variables as those of Figure 1(a). First, it is clear that convergence is achieved for the whole range of field strengths regardless of the approximation used. This happens because the ratio $(\mathcal{E}/(a^*_{00}(1)))^n$ is now finite due to the presence of the effective temperature on the denominator (which varies similarly to the energy $\mathcal{E}$ keeping terms from exploding). The insets of Figure 1(b) show that subsequent approximations overall tend towards the exact value, with the slight fortuity that the first approximation is surprisingly accurate at high fields. While this result is important, the accuracy of the first approximation is only high for the Lorentz case, for which the solution is known exactly, and worsens rapidly for heavier ions. While no exact answer is known for other cases, one can nonetheless test the approximations with respect to each other to arrive at qualitative conclusions. Figure 2 shows the results for the first 4 approximations

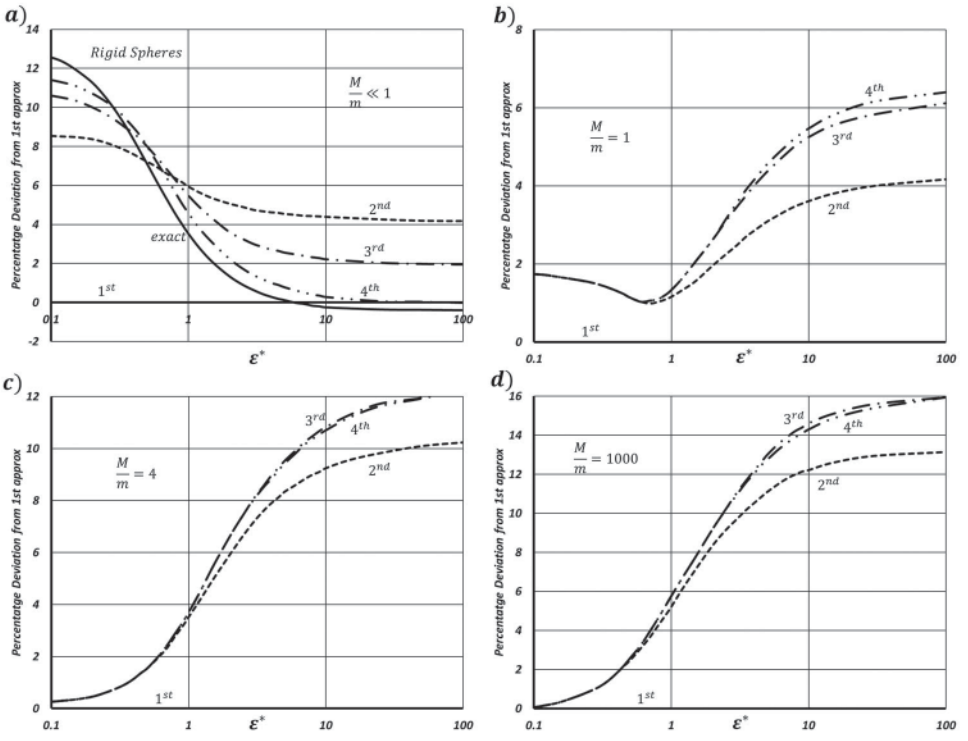

Figure 2. Shows the percentage deviation from the two-temperature theory approximations with respect to the first approximation as a function of the E/n term ε^* for different mass ratios (a) $M/m \ll 1$, (b) $M/m = 1$, (c) $M/m = 4$, (d) $M/m = 1000$.

as a function of different mass ratios M/m and where the y axis is now written as

$$\%\text{deviation from first approximation} = \frac{\langle v_d^* \rangle_X - \langle v_d^* \rangle_I}{\langle v_d^* \rangle_I} \cdot 100$$

where X corresponds to a given approximation [56]. Figure 2(a) is the equivalent result to Figure 1(b) at low ion masses ($M/m \ll 1$). The other three panels in Figure 2 correspond to M/m ratios of 1, 4 and 1000. At first glance, results convey that, as the mass of the ion increases, all approximations become increasingly accurate for small fields. This agrees with the notion that zero field extra terms of α_0 in Equations (7)–(8) and the zero field terms of α^* in Equation (12) are directly proportional to m/M, so that they disappear rather quickly at large ion masses. Contrary to what happens with the Lorentz model, it seems however that the error in the 1st approximation for high fields and large masses worsens considerably. One might naturally expect that the 4th approximation is the most accurate, but Figure 2 shows that the third approximation is within less than 1% of this value for all fields and ions of interest, and the second approximation would be perhaps within 3-4% at most, with the largest deviations occurring only at very high fields. Based on these results, as a practical rule, at least the second approximation of the two-temperature theory should be considered when dealing with small to large masses of ions except for very small fields.

The two-temperature theory suggests that the ion distribution presented in Equation (6) can be modified as follows to account for high fields and small ion masses, at least as a first approximation:

$$F(z_i) = \left(\frac{M}{2\pi k T_{eff}}\right)^{3/2} e^{-\frac{M(z_i - v_{di})^2}{2kT_{eff}}}. \tag{14}$$

Use of Equation (14) to calculate mobility and ion's energy yields Equations (9) and (10) (see appendix A, C). Despite the success of the two-temperature theory, there is an obvious shortcoming. T_{eff} requires the drift velocity to be known, but the drift velocity is a function of T_{eff} through the mobility. This convolution hints at the possibility of an iteration procedure for accurate calculations, but the added difficulty often does not yield sufficient improvement to make it practically useful.

Omitted in the above approximations is the possibility of inelastic collisions for polyatomic entities, as it has been assumed thus far that all collisions are elastic. However, for polyatomic ions, realistic collisions may involve energy transfer to rotational and vibrational degrees of freedom. This effect, or at least a simplification of it, is known as accommodation of the gas molecule to the temperature of the ion and has been explored extensively in the aerosol field (see, for example, Garcia-Ybarra and Rosner and others) [58–60]. This accommodation also assumes that the ion collision is no longer exclusively specular and considers that gas molecules are emitted diffusely. The resulting drag force, F_{Di}, for this consideration, which involves tensors, is given by

$$dF_{Di} = \oint_A \frac{2mn_{gas}}{\sqrt{\pi h}} \left[\left(1 - \frac{3a}{4} + \frac{a\pi}{8}\right)\overline{\overline{nn}} + \frac{a}{4}\bar{\bar{I}}\right] \cdot v_{dj} dA; F_{Di} = B_{ij} v_{dj}, \tag{15a-b}$$

where $\overline{\overline{nn}}$ and $\bar{\bar{I}}$ are the normal and unit dyadics, a is the thermal accommodation coefficient, $h = m/2kT$, and dA is the physical surface area of the ion. When employed for singly charged aerosol particles ($M >> m$) with an accommodation coefficient of 90-91% corresponding to a CCS enhancement of approximately $\sim$1.36 [39], its result has been shown to agree within a few per cent of experimental results [31,61–63]. Although this coefficient may seem arbitrary at first, aside from the accuracy of its result, it likely partially originates from the conversion of kinetic energy in the collisions to internal energy of the ion. It has recently been shown that about 90% of the centre of mass frame collision energy is converted to internal energy when modelling Collision Induced Dissociation [64]. Even though the theoretical quadrature in Equation (15a) does not carry any potential interaction, it can be shown that a numerical alternative to this calculation separating impinging from reemitted gas molecules allows for long range interactions to be taken into account. It is noteworthy to mention that a variation of the Boltzmann equation was proposed for inelastic collisions and polyatomic ions, termed the Wang-Chang-Uhlenbeck-de Boer (WUB) equation, but its use is limited, at least in analytical chemistry, due to the difficulty that the collision dynamics entail [65–67].

A final projection is that, although there have been some further theoretical improvements over the years, such as the three-temperature theory (to improve convergence for diffusion) [67,68], quantum effects (with the largest effect coming from discrete values of the angular-momentum quantum number) [69], or mixtures of gases (a small change in

the moment equations would allow this effect to be incorporated) [70], most ion mobility calculations relevant to analytical chemistry to date can be performed using the above formulas with only modest error ($\sim 10\%$).

3. Numerical approaches to the calculation of ion mobility and collision cross sections.

It should be apparent at this point that, in order to obtain the CCS from Equation (3) or any equivalent description of the gas-ion interaction, a numerical calculation under all but the simplest calculations will be required. In order to do so, one must initially have an all-atom model of the ion. This model may be obtained through molecular dynamics (MD), through ab-initio/Density Functional Theory (DFT) calculations, or structures based on condensed-phase x-ray crystal structures, cryoelectron microscopy data, or NMR data may be used. This model will then be used to obtain the CCS. Many different methods exist, but the most commonly used ones assume two things: (1) The atoms remain fixed in space during the calculation and (2) all the orientations are equally probable. The first simplification neglects vibrations and conformational heterogeneity of the ion as well as any rotational effects (some approaches do attempt to account for conformational heterogeneity by computing a distributions of CCS for static structures sampled from MD simulations [71,72]). Any interchange between translational and rotational/vibrational degrees of freedom is therefore ignored or embedded into a parameter (accommodation) and any secondary effect from vibrations or rotation is also ignored. The second simplification neglects any alignment effect from the field, whether it may come from the ion's permanent dipole or from purely aerodynamic effects. These effects are normally small, so their omission is justified under regular scenarios of small ions (i.e. with dimensions much smaller than the gas mean free path) and low fields. Unless specified directly all methods listed below follow these assumptions.

For the purposes of this review, our discussion in this section revolves mostly around state-of-the-art IM calculations. A list of the most common calculation methods is presented in Table 2. We again separate the discussion between the fields of analytical chemistry and aerosol science, focusing on the former while making emphasis on common ground and consilience. Viehland was one of the pioneers in testing MonteCarlo simulations for polyatomic ions using a simple inelastic model with some success [65]. Interestingly enough, however, the first seemingly accurate result for CCS of tens of atoms was nonetheless obtained by a simple projection approximation (PA) algorithm proposed by Edward Mack in 1925 for gaseous diffusion methods [73]. It was later picked up by Bowers and coworkers [74]. As its name suggests, the calculation involves using a projection or 'shadow' of the ion in different orientations and calculating the area of each shadow using the atom models specified above. Atomic radii used for the projection are generally VdW radii with little to no modification. The results from the basic form of PA are equivalent to ignoring any type of potential interaction and assume, perhaps inadvertently, that the collisions with gas molecules are specular, elastic and without any secondary scattering and, therefore, the resulting CCS would be the same for a solid ion as for a very thin shell with the same exterior. Under this hypothesis, the results from PA should only be reliable for gases with small masses and polarisabilities and for small ions with negligible scattering. Indeed, direct results obtained from PA are only acceptable for small ions under

Table 2. Classification of numerical approaches to CCS and ion mobility.

Projection Approximation Methods	**Projection Approximation (PA) method**. The ion's 'shadow' is projected onto different planes and the projection area orientationally averaged to yield an approximation of the CCS. The atoms and gas molecules (which are incorporated in the projection) use van der Waals radii. **Impact (Ion Mobility Projection Approximation Calculation Tool)**. A PA method that clusters atoms in the ion into cuboidal sections yielding a multilevel octree and improving performance over regular PA. The accuracy is enhanced by using a calibration constant. **PSA (Projected Superposition Algorithm)**. Similar to the PA method but uses a shape factor to account for the concaveness of the ion relative to a purely convex ion of the same size. Other corrections that consider potential interaction are included.	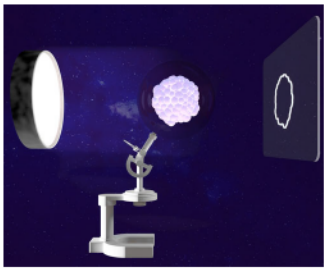
Hard Sphere Scattering Methods	**EHSS (Exact Hard Sphere Scattering)**. Monte Carlo type simulation where gas molecules follow rectilinear trajectories directed towards the ion. The gas molecules are allowed to collide multiple times with the ion before the exiting the domain, and collisions are assumed to be specular and elastic. **DHSS (Diffuse Hard Sphere Scattering)**. Similar to the EHSS calculation above but where the gas molecule instantly accommodates to the surface temperature of the ion. The reflection may be regarded as diffuse and inelastic.	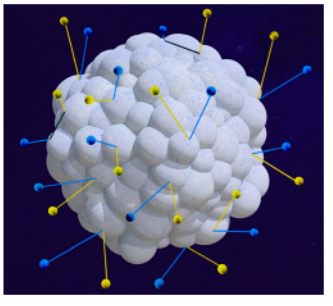
Trajectory Methods	**Trajectory Method (TM)**. The TM method is similar to the EHSS methods, but a potential interaction is used, and gas molecule trajectories are no longer rectilinear. The most common potential interaction used in TM is a Lennard-Jones 4-6-12 law, but Buckingham-type potentials have also been used. For nitrogen environments, an additional ion-quadrupole potential term has been implemented in some approaches. **Trajectory Diffuse Hard Sphere Scattering Method (TDHSS)**. It is similar to the TM method above, but the interaction is instead a $4 - \infty$ law. Collisions can be chosen to be diffuse and inelastic or specular. **Diatomic Trajectory Method (DTM)**. Similar to the TDHSS method, but the rotational degrees of freedom of the nitrogen molecule and the conversion between angular and linear momentum have been taken into account.	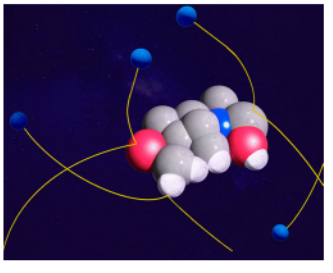
Molecular Dynamics Methods	Full Molecular Dynamics calculations that include the ion and gas molecule interacting through all of their translational, vibrational, and rotational degrees of freedom and where an electrical field must be present.	
Machine Learning Algorithms	**MetCCS**. Makes use of Machine Learning, Databases and Molecular Descriptors to make an informed guess on the value of CCS of previously unknown molecules.	

He environments for which attraction potentials are quite small. Nonetheless, PA can very efficiently compute a CCS approximation, so it is still extensively used, in particular when corrections from other effects are taken into account [75,76].

Soon after Bowers' introduction of PA, Jarrold and co-workers made use of Equation (10) to develop a suite of algorithms, MOBCAL, that would allow the CCS of polyatomic ions to be calculated with surprising accuracy [51,77]. MOBCAL continues, even to this day, to be one of the most widely used tools for these types of calculations. Aside from the PA algorithm, MOBCAL is capable of performing two other types of MonteCarlo calculations with the purpose of obtaining the deflection angle through the use of different types of potential interactions so that Equation (3) (which may incorporate T_{eff} if necessary) may be integrated. The idea behind the algorithm is in reality quite simple: gas molecules that obey the velocity distribution specified in Equation (3) are let lose at different impact parameters (b) towards the ion. The gas then interacts with the ion depending on the potential interaction, and the deflection angle χ is recorded once the gas molecule is sufficiently far from the ion. This is repeated a myriad of times for different impact parameters, relative velocities, and orientations of the ion. Out of the two MonteCarlo calculations, the simplest one is labelled Exact Hard Sphere Scattering (EHSS) which uses a $0 - \infty$ type interaction, and therefore involves rectilinear trajectories together with specular and elastic collisions. The gas trajectories can be subject to multiple collisions with the ion. EHSS yields a very similar value to PA for small ions in He environments but performs better for larger molecules as the scattering effect increases. The second of such calculations is known as the Trajectory Method (TM or TMLJ) which includes Lennard-Jones (L-J) interactions between individual atoms and gas molecules as well as an ion-induced dipole potential. The 4-6-12 potential employed in TMLJ for an ion-gas pair is given by [51]:

$$\Phi(x,y,z) = 4\epsilon \sum_{i=1}^{K} \left[\left(\frac{\sigma}{r_i}\right)^{12} - \left(\frac{\sigma}{r_i}\right)^{6} \right] - \frac{\alpha_p}{2}\left(\frac{ze}{K}\right)^2 \left[\left(\sum_{i=1}^{K} \frac{x_i}{r_i^3}\right)^2 + \left(\sum_{i=1}^{K} \frac{y_i}{r_i^3}\right)^2 + \left(\sum_{i=1}^{K} \frac{z_i}{r_i^3}\right)^2 \right]. \quad (16)$$

$r_i = (x_i, y_i, z_i)$ is the relative distance between each of the K atoms (and/or charges) and the gas molecule, with α_p being the polarisability of the buffer gas, and ϵ and σ are the Lennard-Jones(L-J) gas-atom parameters corresponding to well-depth and zero potential crossing, respectively. Figure 3(a) shows a representation of the calculation of trajectories that depend on the impact parameter b, the relative velocity of the ion and gas particle, and the deflection angle. When this calculation is done for multiple different orientations, Equation (3) may be calculated. When well-calibrated L-J potential pairs are used, CCS predicted with TMLJ agreed quite well with empirically measured ones in He, even when compared at different temperatures. While the TMLJ is extremely successful, the L-J parameters (and polarisabilities) are distinct for each gas-atom pair, thus they need to be separately calculated (or derived from combination rules) for each such pair.

As an increasingly greater number of mobility calculations were performed, it became apparent that a systematic way of optimising L-J parameters is required for optimal mobility calculations, especially for the most used gases, N_2 and He. At the same time, a question remained on whether a 4-6-12 potential was sufficient to study polyatomic gases. Kim and

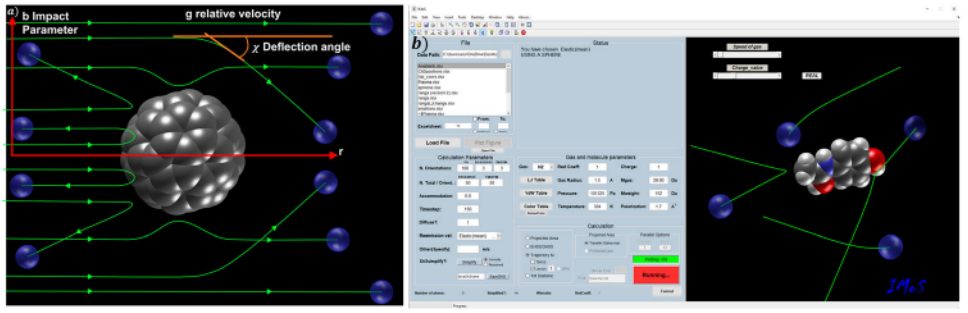

Figure 3. (a)Representation of the calculation done by MOBCAL/Collidoscope to obtain the result to Equation (3) depending on the potential used. (b) IMoS interface with a representation of the calculation using a 4-6-12 forcefield.

co-workers added an ion-quadrupole in order to study mobility in N_2 showing significant promise [78]. However, in their work, Kim et al. used a universal forcefield to assign L-J parameters to N_2, significantly affecting performance. Campuzano et al. used Kim's forcefield but optimised the L-J parameters for organic substances (C, H, O, N, F) showing that numerical calculations could be within 4% of their experimental counterparts for common ions ranging between 70 and 720 Da [6]. In the meantime, calculations performed using EHSS in N_2 failed to give accurate results for any ion size, even when an appropriate gas diameter for N_2 was used [61,79]. A possible reason relies on the questionable validity of specular reemission for heavier gases. This hypothesis is indeed in contrast to the expected inelastic and diffuse reemission that is observed from diffusion and mobility of very large molecules and aerosol particles, and that had been predicted by Millikan, Epstein and even Smoluchowski on gases colliding with surfaces [39,40].

At this point, it is relevant to describe some of the numerical accomplishments of mobility calculations that had been done in parallel for larger charged particles (from tens to hundreds of nm). In the aerosol field, there had been many successful attempts at analytical solutions of electrical mobility, as the particles could be represented by simplified models rather than all-atom structures. However, for particles that differed from geometrically simple structures, such as soot-type fractals, theoretical approaches became intractable. In 1981, Chan and Dahneke used Monte Carlo simulations to study the drag force on chains of spheres taking into account 'parasitic' interactions (i.e. scattering effects) [80]. Other works followed; in particular Mackowski developed an algorithm that would sample gas molecules into a control volume by assuming a skewed Maxwell distribution similar to that of Equation (A.2) in Appendix A [81]. In the algorithm the ion is given an orientation, the distribution is sampled, and gas molecules may enter the domain from any boundary and in any direction much like as a 'physical gas' would, and the drag force is calculated from the momentum transfer of all gas molecules divided by the total physical time it would take to sample them. The trajectories inside the domain are rectilinear, and if the gas molecules collide with the particle, reemission may be assumed to be either elastic or inelastic and either specular or diffuse. The calculation is performed three times in three perpendicular directions, enabling calculation of a symmetric drag tensor. In Mackowski's algorithm, the tensor is averaged through Happel and Brenner's settling velocity theory, however it should

be emphasised that the result is a quantity related to, but different from, the ion mobility and should not be used to interpret IM experiments [53].

Larriba and Hogan expanded on Mackowski's physical gas concept to create IMoS [82–84]. IMoS is a suite of parallelised algorithms for IM computations that allows potential interactions to be incorporated. The interface for this programme appears in Figure 3(b), where an illustration shows how gas molecules appear from all directions, in contrast to how Equation (3) is calculated in MOBCAL. IMoS includes both EHSS and DHSS (Diffuse Hard Sphere Scattering), enabling the use of the accommodation coefficient a, and both inelastic and diffuse collisions are implemented. DHSS yields a better approximation to the CCS in N_2 for larger singly charged particles and provides the 1.36 enhancement factor predicted by Epstein [84]. IMoS users may choose to add an ion-induced dipole potential interaction to the DHSS and EHSS algorithms, resulting in trajectory calculations labelled as TDHSS. The user can also choose to use a 4-6-12 potential interaction similar to that in MOBCAL as well as an ion-quadrupole potential proposed by Kim and coworkers for calculations in N_2. IMoS has optimised some L-J parameters, and it was shown that the ion-quadrupole potential can also be effectively embedded into the L-J parameters without perceptible loss of accuracy [85]. It also has its own version of gas molecule rotation using the moment of inertia of the diatomic nitrogen molecule, implemented as the 'Diatomic Trajectory Method' (DTM), although no perceptible advantage is gained from its addition when compared to the use of an average diameter or parameter [86]. In all, IMoS results differ less than 1% from those of MOBCAL, proving the validity of both suites of algorithms.

A couple of interesting outcomes have been produced using IMoS together with experiments. Most interesting is the confirmation that elastic and specular collisions as well as inelastic and diffuse collisions play important roles in the calculation of CCS [61]. For small ions, gases like He seem to have dominantly elastic and specular interactions while heavier gases like N_2 may be more subject to inelastic and diffuse collisions. As ions become larger (in the kDa-GDa range), either due to multiple scattering at the surfaces, or to stronger dispersion interactions, reemission becomes effectively diffuse, regardless of the gas, matching what is observed for micron sized particles, i.e. $\Omega \sim 1.36PA$ [87–89]. Stemming from this result, one can consider the CCS to be a combination of effects, e.g. $\Omega = \mathcal{L}\xi PA$, where ξ is the accommodation/scattering portion ($\sim$1-1.39), and $\mathcal{L}$ is the enhancement due to grazing and collision effects from interaction potentials.

Other numerical programmes have recently surfaced as a testament to the need to enhance mobility calculations. Collidoscope is a great tool that has parallelised the algorithms in MOBCAL, making its calculations as efficient as those in IMoS [90]. Taking into account that the CCS integral has an inherent geometrical portion, corrections to PA similar to $\mathcal{L}\xi PA$ above have been developed to make efficient predictions to mobility. Among the most widely used are the Ion Mobility Projection Approximation Calculation Tool (IMPACT) [75], which is an impressively fast tool for calculating large all-atom complexes, and the Projected Superposition Approximation (PSA), which includes the calculation of a shape factor reminiscent of the effect of the $\mathcal{L}\xi$ pair [76]. Even more calculators have surfaced as a testament of the necessity of these tools, such as Mobcal-MPI or HPCCS [91,92], with only very minor modifications to the original MOBCAL code that focus on computational efficiency. A recent interesting approach is that of machine learning methods, such as MetCCS, which makes use of molecular descriptors to make predictions on CCS. With

enough data available, it could be the most efficient method for large data sets where very high accuracy ($\sim$1-4%) is not required [93].

4. Future of numerical calculations

The ability of numerical methods to predict ion mobility to within a few per cent should be commended given the complexity of the physical calculation. Nonetheless, with experimental methods improving drastically and reaching accuracies far beyond our current theoretical and numerical capabilities, the necessity of relaxing some of the simplifications to provide better models and understand the separation observed is paramount. The idea behind this section is to showcase a few transcending experimental results in which the above calculations are insufficient, followed by some plausible changes in the algorithms and further developments. Some of these changes are already being considered and should eventually bring corrections to the above theory and increase our confidence in interpreting state-of-the-art IM data.

Over the past decade, the resolution achieved by Ion Mobility instruments has improved more than an order of magnitude with recent experiments showing resolutions ($K/\Delta K$) of over 200 (0.5% confidence error) using different systems together with record-breaking, perhaps still inconsistently, target resolutions of over 1000 (0.1%) [20]. These remarkable resolutions are sufficient to separate extremely small changes in either structures, potential interactions, mass shifts or even dipole alignments, proving the validity of IMS for isomer separation analyses [95]. Among some experiments, noteworthy are those of long Drift Tubes [19], cyclic ion travelling wave devices [96], Trapped Ion Mobility Spectrometry (TIMS) [97,98], Field Asymmetric Waveform Ion Mobility Spectrometers (FAIMS) and Structures for Lossless Ion Manipulations (SLIM) devices [95]. Shvartsburg and coworkers have used FAIMS to separate diglyceride lipids that only differed in the double bond orientation [99]. Moreover, they have shown the ability to fully separate isotopologues and showed peak-broadening effects attributed to isotopomer discrimination [94,100,101]. Figure 4(a) has been extracted directly from their work to see the broadening occurring when either a chloride isotope or a chloride and carbon isotopes are studied instead of the base monochloroaniline. The broadening of the peak can only be attributed to different positions of the heavy carbon isotopes. The SLIM IM board has been shown capable of separating enantiomers using cyclodextrins [102]. More recently, SLIM has been shown to discriminate arginine isotopologues not only through reduced mass shifts in Equation (2) but through distinct additional relative mobility shifts [23]. These shifts seem to be attributed to a change in the centre of mass of the ion due to the different locations of the isotopic mass differential. A tetraalkylsalt study was performed, shown in Figure 4(b) (extracted directly from their work) where the broadening of the peak can only be attributed once again to different positions of the isotopic mass. This was further corroborated through iodoacetyl isotopomer compounds, shown in Figure 4(c) (extracted also from [23]) where the shift maybe perceived in the arrival time.

Most, if not all the separations depicted in the paragraph above, regardless of whether the separation is due to ultra-high resolutions, high-fields, centre of mass shifts, dipole moments, . . . , would either not be separable through any of the above numerical algorithms, or if they are, the separation provided should be critically inspected to make sure that the discrimination observed numerically is the same as the discrimination observed

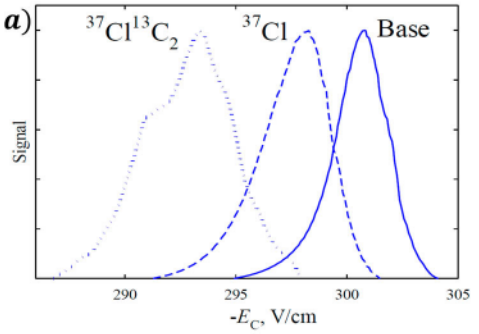

Figure 10. The FAIMS spectra for 2-MCA isotopologues at m/z = 128, 130, and 132 (DV = 5 kV, He 43%). The broadening of $^{37}Cl^{13}C_2$ peak is apparent.

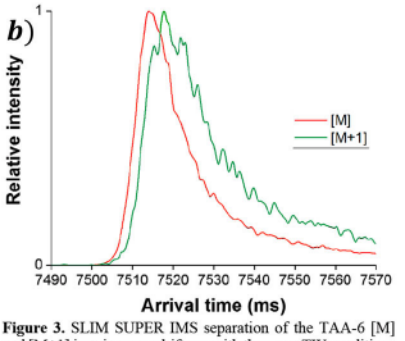

Figure 3. SLIM SUPER IMS separation of the TAA-6 [M] and [M+1] ions in argon drift gas with the same TW conditions as those used in Figure 2 after carefully controlling ion populations to avoid detector saturation for [M] (as evident in Figure 2). The ~25% broader [M+1] peak relative to the [M] peak suggests the possibility of variations in the mobilities of its component isotopomers.

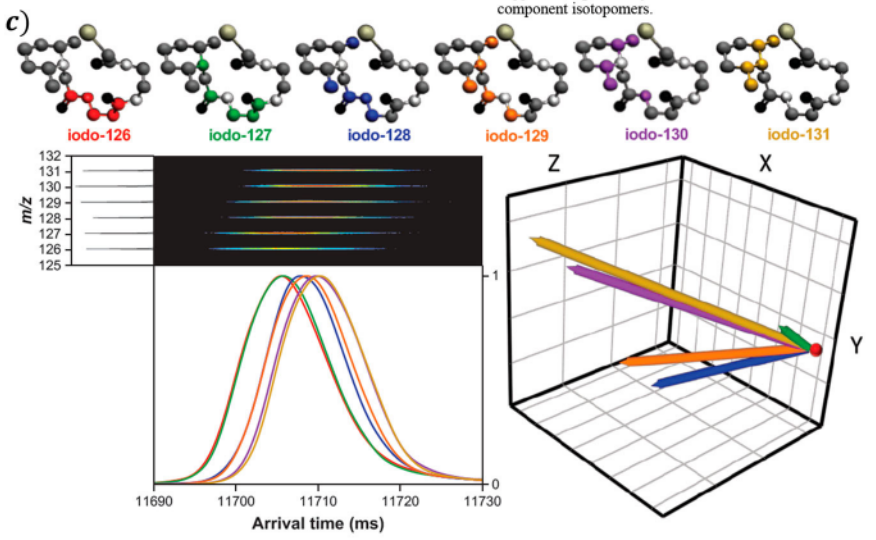

Figure 7. SLIM SUPER IMS separation of a mixture of six iodo-TMT isotopomers in nitrogen drift gas after 1354.5 m. The $[M+H]^+$ parent ion (458 m/z) was fragmented post-SLIM IMS separation to yield non-isobaric reporter ions (126, 127, 128, 129, 130, and 131 m/z) used to construct the arrival time distribution (bottom left), revealing the separation of the six isotopomers. IMS-MS illustration of the fragment ions is also shown (bottom left). CoM vectors (bottom right) relative to the iodo-126 (red dot). 3D structures of the iodo-TMT are displayed (top). Hydrogen atoms were removed for ease of visualization.

Figure 4. Isotopomer separations using (a) FAIMS and (b) (c) SLIM devices. Extracted from refs. (a) [94], (b,c) [23]. Reprinted with permission from Journal of *Analytical Chemistry* [23] and [94]; Copyright © 2019 American Chemical Society.

empirically. In what follows, a clear depiction of the most common difficulties in numerical calculations is enumerated and, when possible, what sort of actions should be performed to relax such simplifications:

(1) *Calculations at higher field to gas density ratios (E/n).* There are plenty of effects that remain unknown when studying mobility toward the high E/n range. Leaving aside possible alignments due to the field, or energy exchanges (addressed below), this point focuses on the additional correction terms required. The Mason-Schamp equation (Equation (2)) cannot be used at higher fields for obvious reasons, and its correction using one-temperature theory terms for Equation (7) is not recommended

except for cases of weak fields. The first approximation to the two-temperature theory (Equation (10)) has been shown in the Lorentz model ($m \gg M$) to yield values within about 12% for E/n up to several hundred Townsends. For other masses, i.e. $M/m \geq 1$, the 1st approximation is adequate for most fields but may incur errors that are unsatisfactory if one is not careful, as can be observed in Figure 2. Despite the difficulty involved in calculating Equation (10), the end result is that, if the effective temperature (T_{eff}) is known, it could be used to approximate the mobility at any field. In fact, MOBCAL, Collidoscope, Mobcal-MPI or IMoS may be used already without any further change to achieve an approximation at higher fields. This is done by doing the calculations at higher temperatures for the CCS and assuming that the higher temperature refers to the effective temperature and not the temperature of the gas. Figure 5 uses IMoS to calculate the mobility at different E/n for small molecules in He as a function of the reduced mobility $K_0 = \frac{p}{p_0}\frac{T_0}{T}K$. These results are then compared to the empirical results from Albritton and coworkers [103,104]. The accuracy of the result, without any L-J potential modification, is almost shocking for a programme intended for zero field calculations. The accuracy decays at increasingly high fields as is expected and where additional correction terms may be added by using Equation (12) or higher approximations. Interestingly enough, these results are able to predict all the different types of behaviour proposed for FAIMS [105,106], e.g. whether the reduced mobility increases or decreases with the field, and even an explanation for the behaviours can

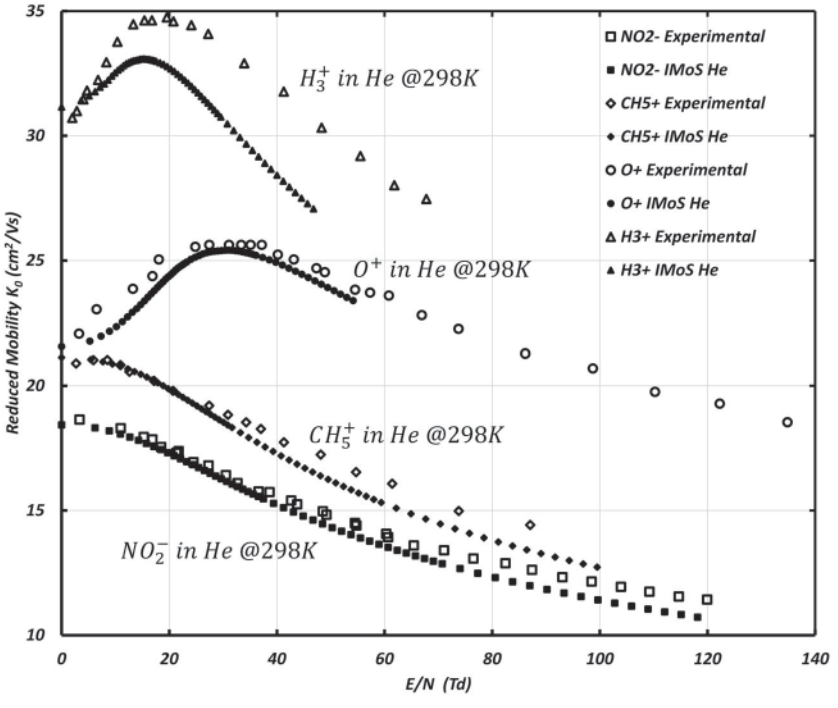

Figure 5. Reduced mobility as a function of E/n for small ions in He. Shown are experimental results obtained from [103,104] together with calculations done with IMoS. The L-J parameters were unmodified from ref. [6].

be extracted. Although it would seem from Figure 2 that the accuracy should be better for H_3^+ than for the rest, one has to take into account that one could optimise the L-J potentials so that the matching is greatly improved (see below).

(2) *Calculations at variable temperature.* While the Mason-Schamp Equation (2) explicitly accounts for temperature, the contribution of temperature to the CCS is many times not addressed experimentally, even though its effect may be quite important, as observed from experiments that have taken into account temperature variations [5,51,107–113]. From a numerical methods perspective, the calculations performed for CCS at higher temperatures (higher T) are no different from those for higher fields (higher T_{eff}). While the CCS is the same, the ion mobility results must in principle be different because, for instance, the gas concentration n itself varies with temperature, yielding different results if T vs. T_{eff} is employed in Equation (12). While the effect of concentration could be avoided by reporting reduced mobilities, other secondary phenomena could complicate the picture. For example, inelastic collisions, which are not accounted for in most numerical calculations, could behave differently at high temperature and high fields. In fact, Viehland compared experimental reduced mobilities for equivalent T and T_{eff} studies in heavy gases such as nitrogen [107]. His studies revealed that the observed reduced mobilities yielded different results, in particular for higher temperatures and very small ions, e.g. NO_x^-. Viehland argued that the difference stemmed from the effects of inelastic collisions occurring at high temperatures that were not present for high fields.

(3) *Determination of mobility-optimised Lennard-Jones parameters and embedding of other effects.* Unfortunately, while there are many numerical mobility calculation methods available, the variations between systems, parameters used, temperatures, and pressures make it difficult to systematically optimise Lennard-Jones parameters. This is even more problematic when some of the effects of other simplifications (inelastic collisions, ion-dipole and ion-quadrupole potentials, ...) may be effectively embedded inside the L-J parameters. Thus only a few optimisation algorithms and results have been systematically proposed [6,85,114,115]. To provide L-J for more than the most common gases and atoms, a standardised technique for the calculation needs to be proposed. Most likely, the study should involve small and large molecules and should focus on isolating outliers (ions with large dipole moments, flat molecules, malleable ions) to determine accurate parameters.

(4) *Effects of inelastic collisions.* Even though numerical and theoretical tools are available to account for the accommodation occurring from inelastic collisions (see Equation (15)), the value of the accommodation is not known except perhaps asymptotically for large ions and heavy gases. This accommodation effect is completely ignored in Equation (3) or any such related collision integral equation. To get accurate solutions in heavier gases like N_2, where some accommodation must occur for many ions, some numerical calculations have embedded the effect into L-J parameters [61]. This has been quite successful, but it is likely that, nevertheless, some error is incurred. For inelastic collisions to be studied in detail, vibrations and rotations must be incorporated into the calculation using molecular dynamics (MD), electron-gas models [116], or quantum mechanics (QM) to accurately model energy exchange [117]. Semiclassical and quantum approaches have been included in variations of the Boltmann equation, such as the WUB equation and its variants [65–67], but no reliable numerical

calculators stemming from these equations exist to date for analytical chemists. In the presence of medium-high fields, it is expected that the energy of the collision should also increase the temperature of the ion, an effect that should qualitatively agree with Wannier's modified formula (adding an inelastic collision similar to the one introduced by Viehland addressed in point 2 [107]) and with the effective temperature of the two-temperature approximation, but which might perhaps lead to deformations of the ion which are not accounted for.

(5) *Speed of angular rotation and effect of the moment of inertia.* Tied to the above simplification, for the aforementioned calculations, the ion remains fixed in space when numerical calculations are performed. Any effect that would come from the speed of rotation is not considered, e.g. effects of different position of the centre of mass due to ion conformation or isotope configuration. Upon a collision, the speed of rotation will be determined by the moment of inertia of the molecule, thus ions with the same molecular structure but very large disparity in the moment of inertia may be separable using ion mobility [118].

(6) *Separation due to permanent dipole moments.* There are two effects in play with dipole moments: (1) charge symmetry vs. structure symmetry, and (2) preferential alignment. The first effect comes into play with highly polarisable gases (mostly N_2 and CO_2) and very non-symmetric molecules with large dipole moments. For those cases, the position of the charges will have an effect even when all orientations are equally probable. This effect allows separation of ions based on polarisability using different gases, among which CO_2 is particularly notable [119,120]. For the latter effect, one must note that when Equation (3) is numerically calculated, it is assumed that no alignment exists. This condition must be relaxed together with (4) for the dipole alignment effect to be considered fully as a function of the field.

(7) *Large particles and/or high fields: beyond the free molecular regime.* As very high fields are encountered, the high velocities acquired by the ion may perturb the centre-of-mass-frame gas velocity distribution, invalidating the assumption of a Maxwell–Boltzmann distribution for the gas. This is also true as the size of the ion approaches the mean free path. Whether it is the ion size, the field strength, or a mixture of both, there will be a point where the free molecular condition can no longer be satisfied and the ion is considered to be in the transition regime, where the theoretical framework described above is no longer be valid. There is some empirico-numerical work in the transition regime with the empirical Stokes-Millikan equation and the Cunningham correction factor [37,40,121].

(8) *Other effects.* Effects such as compaction of ions structure upon transfer from aqueous solution to the gas phase [122,123], molecule flexibility, gas geometry or gas molecule rotation, quadrupole or higher-order moments, quantum effects, and aerodynamic alignments, which are typically minor under most scenarios, could perhaps become prominent in particular cases. If possible, and with critical insight, some of these effects may perhaps be embedded into other parameters that allow computation of the CCS without significant loss of accuracy.

Comprehensively, many of these effects are now being taken into account in second generation calculators. For example, many algorithms now include MD to calculate transport properties [124–126]. A second-generation calculator, IMoS 2.0, is being developed

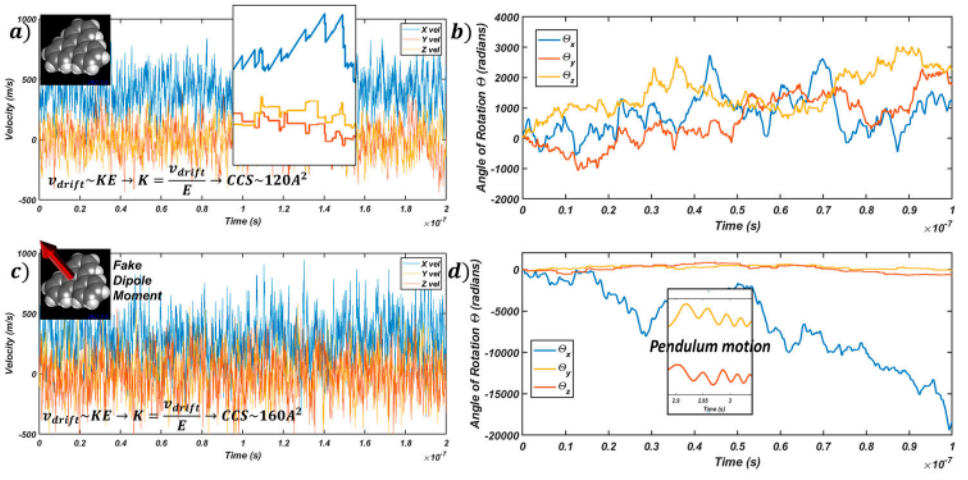

Figure 6. Numerical results obtained from a simulation of an ion inside a physical gas subject to an electric field in the x direction. The ion has fixed atoms but may freely rotate and slow down (or speed up) with each collision. (a and c) show the velocity of the ion in all three coordinates as a function of time with the difference that (a) has no dipole moment while (c) has a strong dipole moment. (b and d) show the angle of orientation of the ion as a function of time for the same cases as (a and c) respectively.

as shown in Figure 6. This algorithm explores the drift-diffusion of an ion in a modelled gas that is subject to an arbitrary field in three dimensions. The ion's orientation, angular velocity and drift velocity become subject of the gas/ion collisions, the moment of inertia, the reduced mass, the strength of the field, and the position of the charges within the ion. Eventually, the ion reaches an equilibrium drift velocity which through non-linearised theory can now be used to establish the mobility and CCS of the ion. Finally, vibration and translation of the atoms within the ion can be modelled to explore multiple configurations. To test the algorithm, Figure 6(a and b) show the trypheniline molecule (with atoms fixed, although this can be modified to allow motion via MD), as it is accelerated by the field. Collisions with the gas slow down the ion in the lab frame, as predicted [127] and as is shown in Figure 6(a) with the field along the x direction. The moment of inertia and angular-momentum conservation of the ion make it rotate upon collision about the angle shown in Figure 6(b). Given the rotation axes of the ion in Figure 6(b), it is safe to assume that all angles are equally probable for this ion as predicted by Equation (3). With sufficient simulation time, a drift velocity may be extracted and a mobility or a CCS calculated while the velocities in the y and z direction average to zero. As an experiment, one can impose a hypothetical dipole moment of 100 Debye at 15 Townsends with the direction as shown in Figure 6(c). This has the effect of imposing an orientation on the molecule as shown in Figure 6(d), resulting in a much slower drift velocity and two constrained orientations that slightly swing like a pendulum around the equilibrium position. Although not as efficient as the previous algorithms (due to the difficulty imposed by new calculations), these types of calculators are expected to overcome some of the issues of preexisting calculators.

IMoS 2.0 algorithm has been recently shown to separate the isotopomers described in Figure 4(c). The separation occurs through the combination of different angular velocities

of the isotopomers together with distinctive angular to linear momentum exchanges due to the shifts in moments of inertia [128].

5. Conclusions

This manuscript is an effort to consolidate into one work an abridged summary of the most relevant theoretical work pertaining to ion mobility within the free molecular regime. The purpose of such an effort has been to critically outline the simplifications performed to arrive at the different approximations and what must ensue to avoid overreaching when describing the results of numerical calculations. The most prominent ion mobility calculators used nowadays are indeed impressively accurate and they are able to calculate the drift velocity of nanometer-sized ions with errors of only a few per cent for most ions and in seconds to minutes. To ensure that this continues to be the case as experimental systems improve, it is necessary to fully understand existing simplifications and operate in a critical manner, relaxing some of the restrictions if required.

In all, Ion Mobility Spectrometry is in its process of reaching maturity and has become ubiquitous in the field of analytical chemistry. The development of more accurate techniques is expected to continue with no foreseeable limit. Theoretical and numerical tools must continue to evolve together with experimental techniques in order to understand the observed gas-phase separation. Challenges remain and will continue to arise, together with new solutions which will undoubtedly continue to improve IM further.

Acknowledgements

Carlos Larriba-Andaluz would like to acknowledge that this material is based in part upon work supported by the National Science Foundation Division of Chemistry under grant number 1904879 (Program officer Dr. Kelsey Cook); and Kanomax Holdings USA under Grant 4595587. The authors would also like to thank Elena Larriba-Andaluz and Xi Chen for the creation of several figures.

Disclosure statement

No potential conflict of interest was reported by the author(s).

Funding

Carlos Larriba-Andaluz would like to acknowledge that this material is based in part upon work supported by the National Science Foundation Division of Chemistry under grant number 1904879 (Program officer Dr. Kelsey Cook); and Kanomax Holdings USA under Grant 4595587.

ORCID

Carlos Larriba-Andaluz http://orcid.org/0000-0003-0864-7733

References

[1] J. Happel and H. Brenner, *Low Reynolds Number Hydrodynamics: with Special Applications to Particulate Media* (Springer Science & Business Media, Boston, 2012).
[2] Mason, E.A., McDaniel, E.W., Transport properties of ions in gases. NASA STI/Recon Technical Report A. 89, (1988).
[3] C.H. Kruger and W. Vincenti, *Introduction to Physical gas Dynamics* (Wiley, New York, 1965).

[4] McDaniel, E.W., Mason, E.A., *Mobility and Diffusion of Ions in Gases*. (John Wiley and Sons, New York, 1973)
[5] V. Gabelica and E. Marklund, Fundamentals of ion mobility spectrometry. Curr Opin Chem Biol. **42**, 51–59 (2018). doi:10.1016/j.cbpa.2017.10.022
[6] I. Campuzano, M.F. Bush, C.V. Robinson, C. Beaumont, K. Richardson, H. Kim and H.I. Kim, Structural characterization of drug-like compounds by ion mobility mass spectrometry: comparison of theoretical and experimentally derived nitrogen collision cross sections. Anal Chem. **84**, 1026–1033 (2012). doi:10.1021/ac202625t
[7] J.C. May, C.B. Morris and J.A. McLean, Ion mobility collision cross section compendium. Anal Chem. **89**, 1032–1044 (2017). doi:10.1021/acs.analchem.6b04905
[8] L.S. Fenn and J.A. McLean, Biomolecular structural separations by ion mobility–mass spectrometry. Anal Bioanal Chem. **391**, 905–909 (2008). doi:10.1007/s00216-008-1951-x
[9] J.C. May, C.R. Goodwin, N.M. Lareau, K.L. Leaptrot, C.B. Morris, R.T. Kurulugama, A. Mordehai, C. Klein, W. Barry and E. Darland, Conformational ordering of biomolecules in the gas phase: nitrogen collision cross sections measured on a prototype high resolution drift tube ion mobility-mass spectrometer. Anal Chem. **86**, 2107–2116 (2014). doi:10.1021/ac4038448
[10] N.L. Zakharova, C.L. Crawford, B.C. Hauck, J.K. Quinton, W.F. Seims, H.H. Hill Jr and A.E. Clark, An assessment of computational methods for obtaining structural information of moderately flexible biomolecules from ion mobility spectrometry. J Am Soc Mass Spectr. **23**, 792–805 (2012). doi:10.1007/s13361-012-0339-5
[11] S.M. Stow, T.J. Causon, X. Zheng, R.T. Kurulugama, T. Mairinger, J.C. May, E.E. Rennie, E.S. Baker, R.D. Smith and J.A. McLean, An interlaboratory evaluation of drift tube ion mobility–mass spectrometry collision cross section measurements. Anal Chem. **89**, 9048–9055 (2017). doi:10.1021/acs.analchem.7b01729
[12] M. Hernández-Mesa, V. D'Atri, G. Barknowitz, M. Fanuel, J. Pezzatti, N. Dreolin, D. Ropartz, F. Monteau, E. Vigneau and S. Rudaz, Interlaboratory and Interplatform study of Steroids collision cross section by Traveling wave Ion mobility Spectrometry. Anal Chem. **92**, 5013–5022 (2020). doi:10.1021/acs.analchem.9b05247
[13] C. Wu, W.F. Siems, G.R. Asbury and H.H. Hill, Electrospray ionization high-resolution ion mobility spectrometry— mass spectrometry. Anal Chem. **70**, 4929–4938 (1998). doi:10.1021/ac980414z
[14] R. Wojcik, I.K. Webb, L. Deng, S.V. Garimella, S.A. Prost, Y.M. Ibrahim, E.S. Baker and R.D. Smith, Lipid and glycolipid isomer analyses using ultra-high resolution ion mobility spectrometry separations. Int J Mol Sci. **18**, 183 (2017). doi:10.3390/ijms18010183
[15] P. Benigni, C.J. Thompson, M.E. Ridgeway, M.A. Park and F. Fernandez-Lima, Targeted high-resolution ion mobility separation coupled to ultrahigh-resolution mass spectrometry of endocrine disruptors in complex mixtures. Anal Chem. **87**, 4321–4325 (2015). doi:10.1021/ac504866v
[16] A.A. Shvartsburg and R.D. Smith, Ultrahigh-resolution differential ion mobility spectrometry using extended separation times. Anal Chem. **83**, 23–29 (2011). doi:10.1021/ac102689p
[17] L. Deng, I.K. Webb, S.V. Garimella, A.M. Hamid, X. Zheng, R.V. Norheim, S.A. Prost, G.A. Anderson, J.A. Sandoval and E.S. Baker, Serpentine ultralong path with extended routing (SUPER) high resolution traveling wave ion mobility-MS using structures for lossless ion manipulations. Anal Chem. **89**, 4628–4634 (2017). doi:10.1021/acs.analchem.7b00185
[18] M. Amo-González and S. Pérez, Planar differential mobility analyzer with a resolving power of 110. Anal Chem. **90**, 6735–6741 (2018). doi:10.1021/acs.analchem.8b00579
[19] X. Chen, S.A. Raab, T. Poe, D.E. Clemmer and C. Larriba-Andaluz, Determination of gas-phase ion structures of locally polar homopolymers through high-resolution ion mobility spectrometry–mass spectrometry. J Am Soc Mass Spectr. **30**, 905–918 (2019). doi:10.1007/s13361-019-02184-9
[20] R.S. Glaskin, M.A. Ewing and D.E. Clemmer, Ion trapping for ion mobility spectrometry measurements in a cyclical drift tube. Anal Chem. **85**, 7003–7008 (2013). doi:10.1021/ac4015066

[21] P. Dwivedi, C. Wu, L.M. Matz, B.H. Clowers, W.F. Siems and H.H. Hill, Gas-phase chiral separations by ion mobility spectrometry. Anal Chem. **78**, 8200–8206 (2006). doi:10.1021/ac0608772

[22] A.A. Shvartsburg, D.E. Clemmer and R.D. Smith, Isotopic effect on ion mobility and separation of isotopomers by high-field ion mobility spectrometry. Anal Chem. **82**, 8047–8051 (2010). doi:10.1021/ac101992d

[23] R. Wojcik, G. Nagy, I.K. Attah, I.K. Webb, S.V. Garimella, K.K. Weitz, A. Hollerbach, M.E. Monroe, M.R. Ligare and F.F. Nielson, SLIM Ultrahigh resolution Ion mobility Spectrometry separations of isotopologues and isotopomers Reveal mobility shifts due to mass distribution changes. Anal Chem. **91**, 11952–11962 (2019). doi:10.1021/acs.analchem.9b02808

[24] M. Šala, M. Lísa, J.L. Campbell and M. Holčapek, Determination of triacylglycerol regioisomers using differential mobility spectrometry. Rapid Commun Mass Sp. **30**, 256–264 (2016). doi:10.1002/rcm.7430

[25] N. Kuhnert, G.H. Yassin, R. Jaiswal, M.F. Matei and C.H. Grün, Differentiation of prototropic ions in regioisomeric caffeoyl quinic acids by electrospray ion mobility mass spectrometry. Rapid Commun Mass Sp. **29**, 675–680 (2015). doi:10.1002/rcm.7151

[26] A.T. Kirk, C.-R. Raddatz and S. Zimmermann, Separation of isotopologues in ultra-high-resolution ion mobility spectrometry. Anal Chem. **89**, 1509–1515 (2017). doi:10.1021/acs.analchem.6b03300

[27] C.J. Hogan Jr and J.F. De La Mora, Tandem ion mobility-mass spectrometry (IMS-MS) study of ion evaporation from ionic liquid-acetonitrile nanodrops. Phys Chem Chem Phys. **11**, 8079–8090 (2009). doi:10.1039/b904022f

[28] J. Rus, D. Moro, J.A. Sillero, J. Royuela, A. Casado, F. Estevez-Molinero and J.F. de la Mora, IMS–MS studies based on coupling a differential mobility analyzer (DMA) to commercial API–MS systems. Int J Mass Spectrom. **298**, 30–40 (2010). doi:10.1016/j.ijms.2010.05.008

[29] B.K. Ku and J.F. de la Mora, Relation between electrical mobility, mass, and size for nanodrops 1–6.5 nm in diameter in air. Aerosol Sci Tech. **43**, 241–249 (2009). doi:10.1080/02786820802590510

[30] G.A. Eiceman, Z. Karpas and H.H. Hill Jr, *Ion Mobility Spectrometry* (CRC press, Boca Raton, FL, 2013).

[31] J.F. de la Mora, L. de Juan, T. Eichler and J. Rosell, Differential mobility analysis of molecular ions and nanometer particles. TrAC, Trends Anal Chem. **17**, 328–339 (1998). doi:10.1016/S0165-9936(98)00039-9

[32] G.H. Wannier, Motion of gaseous ions in strong electric fields. The Bell System Technical Journal. **32**, 170–254 (1953). doi:10.1002/j.1538-7305.1953.tb01426.x

[33] G.H. Wannier, Motion of gaseous ions in a strong electric field. II. Phys Rev. **87**, 795 (1952).doi:10.1103/PhysRev.87.795

[34] E. Vogt and G.H. Wannier, Scattering of ions by polarization forces. Phys Rev. **95**, 1190 (1954). doi:10.1103/PhysRev.95.1190

[35] J.C. Maxwell, V. Illustrations of the dynamical theory of gases.—part I. On the motions and collisions of perfectly elastic spheres. The London, Edinburgh, and Dublin Philosophical Magazine and Journal of Science. **19**, 19–32 (1860). doi:10.1080/14786446008642818

[36] M.P. Langevin, Ann. Chim. Phys. 5, 245 (1905), translated in E. W. McDaniel, *Collision Phenomena in Ionized Gases* (Wiley, New York, 1964), Appendix II.

[37] E. Cunningham, On the velocity of steady fall of spherical particles through fluid medium. Proceedings of the Royal Society of London. Series A, Containing Papers of a Mathematical and Physical Character. **83**, 357–365 (1910).

[38] P. Lenard, W. Weick and H.F. Mayer, Über Elektrizitätsleitung durch freie Elektronen und Träger. III: Wanderungsgeschwindigkeit kraftgetriebener Partikel in reibenden Medien, mit Beiträgen von W. Weick und Hans Ferd. Mayer. Annalen der Physik. **366**, 665–741 (1920). doi:10.1002/andp.19203660802

[39] P.S. Epstein, On the resistance experienced by spheres in their motion through gases. Phys Rev. **23**, 710 (1924). doi:10.1103/PhysRev.23.710

[40] R.A. Millikan, Coefficients of slip in gases and the law of reflection of molecules from the surfaces of solids and liquids. Phys Rev. **21**, 217 (1923). doi:10.1103/PhysRev.21.217
[41] S.G. Brush, *Kinetic Theory: Irreversible Processes* (Elsevier, London, 2016).
[42] J.C. Maxwell, Iv. on the dynamical theory of gases. Philosophical Transactions of the Royal Society of London **157**, 49–88 (1867).
[43] S. Chapman, T.G. Cowling and D. Burnett, *The Mathematical Theory of non-Uniform Gases: an Account of the Kinetic Theory of Viscosity, Thermal Conduction and Diffusion in Gases* (Cambridge University Press, New York, 1990).
[44] H.X. Hassé, Langevin's theory of ionic mobility. The London, Edinburgh, and Dublin Philosophical Magazine and Journal of Science. **1**, 139–160 (1926). doi:10.1080/14786442608633618
[45] H. Hassé and W.L. Cook, The calculation of the mobility of monomolecular ions. The London, Edinburgh, and Dublin Philosophical Magazine and Journal of Science. **12**, 554–566 (1931). doi:10.1080/14786443109461832
[46] Loeb, L.B., *Basic Processes of Gaseous Electronics*. (1955)
[47] A.M. Tyndall, *The Mobility of Positive Ions in Gases* (The University Press, Cambridge, 1938).
[48] Massey, H.S.W., Burhop, E.H.S., Gilbody, H.B., Electronic and ionic impact phenomena. Vols. 1, 2 and 3 (Oxford University Press, Oxford, 1973).)
[49] T. Kihara, The mathematical theory of electrical discharges in gases. B. velocity-distribution of positive ions in a static field. Rev Mod Phys. **25**, 844 (1953). doi:10.1103/RevModPhys.25.844
[50] E.A. Mason and H.W. Schamp Jr, Mobility of gaseous lons in weak electric fields. Ann Phys. **4**, 233–270 (1958). doi:10.1016/0003-4916(58)90049-6
[51] M. Mesleh, J. Hunter, A. Shvartsburg, G.C. Schatz and M. Jarrold, Structural information from ion mobility measurements: effects of the long-range potential. J Phys Chem. **100**, 16082–16086 (1996). doi:10.1021/jp961623v
[52] L. Rayleigh, LIII. Dynamical problems in illustration of the theory of gases. The London, Edinburgh, and Dublin Philosophical Magazine and Journal of Science. **32**, 424–445 (1891). doi:10.1080/14786449108620207
[53] C. Larriba-Andaluz, M. Nahin and V. Shrivastav, A contribution to the amaranthine quarrel between true and average electrical mobility in the free molecular regime. Aerosol Sci Tech. **51**, 887–895 (2017). doi:10.1080/02786826.2017.1316829
[54] H. Skullerud, On the relation between the diffusion and mobility of gaseous ions moving in strong electric fields. J Phys B At Mol Phys. **9**, 535 (1976). doi:10.1088/0022-3700/9/3/021
[55] E. Mason and H.S. Hahn, Ion drift velocities in gaseous mixtures at arbitrary field strengths. Phys Rev A. **5**, 438 (1972). doi:10.1103/PhysRevA.5.438
[56] L.A. Viehland and E. Mason, Gaseous ion mobility and diffusion in electric fields of arbitrary strength. Ann Phys. **110**, 287–328 (1978). doi:10.1016/0003-4916(78)90034-9
[57] L.A. Viehland and E. Mason, Gaseous lon mobility in electric fields of arbitrary strength. Ann Phys. **91**, 499–533 (1975). doi:10.1016/0003-4916(75)90233-X
[58] P. Garcia-Ybarra and D.E. Rosner, Thermophoretic properties of nonspherical particles and large molecules. Aiche J. **35**, 139–147 (1989). doi:10.1002/aic.690350115
[59] J. Fernández de la Mora, Free-molecule mobility of polyhedra and other convex hard-bodies. J Aerosol Sci. **33**, 477–489 (2002). doi:10.1016/S0021-8502(01)00186-0
[60] Z. Li and H. Wang, Drag force, diffusion coefficient, and electric mobility of small particles. I. theory applicable to the free-molecule regime. Phys Rev E. **68**, 061206 (2003). doi:10.1103/PhysRevE.68.061206
[61] C. Larriba-Andaluz, J. Fernandez-Garcia, M.A. Ewing, C.J. Hogan and D.E. Clemmer, Gas molecule scattering & ion mobility measurements for organic macro-ions in He versus N 2 environments. Phys Chem Chem Phys. **17**, 15019–15029 (2015). doi:10.1039/C5CP01017A
[62] Z. Li and H. Wang, Drag force, diffusion coefficient, and electric mobility of small particles. II. application. Phys Rev E. **68**, 061207 (2003). doi:10.1103/PhysRevE.68.061207
[63] B.N. Wahi and B.Y. Liu, The mobility of polystyrene latex particles in the transition and the free molecular regimes. J Colloid Interf Sci. **37**, 374–381 (1971). doi:10.1016/0021-9797(71)90305-5

[64] M.T. Donor, A.M. Mroz and J.S. Prell, Experimental and theoretical investigation of overall energy deposition in surface-induced unfolding of protein ions. Chem Sci. **10**, 4097–4106 (2019). doi:10.1039/C9SC00644C

[65] L. Viehland, S. Lin and E. Mason, Kinetic theory of drift-tube experiments with polyatomic species. Chem Phys. **54**, 341–364 (1981). doi:10.1016/0301-0104(81)85111-7

[66] G.E. Uhlenbeck and J. De Boer, *Studies in Statistical Mechanics* (North-Holland, New York, 1962).

[67] K. Kumar, Matrix elements of the Boltzmann collision operator in a basis determined by an anisotropic Maxwellian weight function including drift. Aust J Phys. **33**, 449–468 (1980). doi:10.1071/PH800449b

[68] L.A. Viehland, Interaction potentials for the alkali ion—rare-gas systems. Chem Phys. **85**, 291–305 (1984). doi:10.1016/0301-0104(84)85040-5

[69] H.T. Wood, General expression for the quantum transport cross sections. J Chem Phys. **54**, 977–979 (1971). doi:10.1063/1.1675028

[70] C.N. Naylor, T. Reinecke and B.H. Clowers, Assessing the impact of drift Gas polarizability in polyatomic Ion mobility experiments. Anal Chem. **92**, 4226–4234 (2020). doi:10.1021/acs.analchem.9b04468

[71] F.C. Liu, T.C. Cropley, M.E. Ridgeway, M.A. Park and C. Bleiholder, Structural analysis of the glycoprotein complex avidin by tandem-trapped ion mobility spectrometry–mass spectrometry (tandem-TIMS/MS). Anal Chem. **92**, 4459–4467 (2020). doi:10.1021/acs.analchem.9b05481

[72] C. Bleiholder and F.C. Liu, Structure relaxation approximation (sra) for elucidation of protein structures from ion mobility measurements. J Phys Chem B. **123**, 2756–2769 (2019). doi:10.1021/acs.jpcb.8b11818

[73] E. Mack Jr, Average cross-sectional areas of molecules by gaseous diffusion methods. J Am Chem Soc. **47**, 2468–2482 (1925). doi:10.1021/ja01687a007

[74] G. Von Helden, M.T. Hsu, P.R. Kemper and M.T. Bowers, Structures of carbon cluster ions from 3 to 60 atoms: Linears to rings to fullerenes. J Chem Phys. **95**, 3835–3837 (1991). doi:10.1063/1.460783

[75] E.G. Marklund, M.T. Degiacomi, C.V. Robinson, A.J. Baldwin and J.L. Benesch, Collision cross sections for structural proteomics. Structure. **23**, 791–799 (2015). doi:10.1016/j.str.2015.02.010

[76] C. Bleiholder, T. Wyttenbach and M.T. Bowers, A novel projection approximation algorithm for the fast and accurate computation of molecular collision cross sections (I). method. Int J Mass Spectrom. **308**, 1–10 (2011). doi:10.1016/j.ijms.2011.06.014

[77] A.A. Shvartsburg and M.F. Jarrold, An exact hard-spheres scattering model for the mobilities of polyatomic ions. Chem Phys Lett. **261**, 86–91 (1996). doi:10.1016/0009-2614(96)00941-4

[78] H. Kim, H.I. Kim, P.V. Johnson, L.W. Beegle, J. Beauchamp, W.A. Goddard and I. Kanik, Experimental and theoretical investigation into the correlation between mass and ion mobility for choline and other ammonium cations in N2. Anal Chem. **80**, 1928–1936 (2008). doi:10.1021/ac701888e

[79] D. Canzani, K.J. Laszlo and M.F. Bush, Ion mobility of proteins in nitrogen gas: effects of charge state, charge distribution, and structure. J Phys Chem A. **122**, 5625–5634 (2018). doi:10.1021/acs.jpca.8b04474

[80] P. Chan and B. Dahneke, Free-molecule drag on straight chains of uniform spheres. J Appl Phys. **52**, 3106–3110 (1981). doi:10.1063/1.329173

[81] D.W. Mackowski, Monte Carlo simulation of hydrodynamic drag and thermophoresis of fractal aggregates of spheres in the free-molecule flow regime. J Aerosol Sci. **37**, 242–259 (2006). doi:10.1016/j.jaerosci.2004.11.011

[82] C. Larriba and C.J. Hogan Jr, Ion mobilities in diatomic gases: measurement versus prediction with non-specular scattering models. J Phys Chem A. **117**, 3887–3901 (2013). doi:10.1021/jp312432z

[83] C. Larriba and C.J. Hogan Jr, Free molecular collision cross section calculation methods for nanoparticles and complex ions with energy accommodation. J Comput Phys. **251**, 344–363 (2013). doi:10.1016/j.jcp.2013.05.038
[84] V. Shrivastav, M. Nahin, C.J. Hogan and C. Larriba-Andaluz, Benchmark comparison for a multi-processing ion mobility calculator in the free molecular regime. J Am Soc Mass Spectr. **28**, 1540–1551 (2017). doi:10.1007/s13361-017-1661-8
[85] T. Wu, J. Derrick, M. Nahin, X. Chen and C. Larriba-Andaluz, Optimization of long range potential interaction parameters in ion mobility spectrometry. J Chem Phys. **148**, 074102 (2018). doi:10.1063/1.5016170
[86] C. Larriba-Andaluz and C.J. Hogan Jr, Collision cross section calculations for polyatomic ions considering rotating diatomic/linear gas molecules. J Chem Phys. **141**, 194107 (2014). doi:10.1063/1.4901890
[87] D.J. Rader, Momentum slip correction factor for small particles in nine common gases. J Aerosol Sci. **21**, 161–168 (1990). doi:10.1016/0021-8502(90)90001-E
[88] M.D. Allen and O.G. Raabe, Slip correction measurements of spherical solid aerosol particles in an improved Millikan apparatus. Aerosol Sci Tech. **4**, 269–286 (1985). doi:10.1080/02786828508959055
[89] T. Wyttenbach, C. Bleiholder and M.T. Bowers, Factors contributing to the collision cross section of polyatomic ions in the kilodalton to gigadalton range: application to ion mobility measurements. Anal Chem. **85**, 2191–2199 (2013). doi:10.1021/ac3029008
[90] S.A. Ewing, M.T. Donor, J.W. Wilson and J.S. Prell, Collidoscope: an improved tool for computing collisional cross-sections with the trajectory method. J Am Soc Mass Spectr. **28**, 587–596 (2017). doi:10.1007/s13361-017-1594-2
[91] C. Ieritano, J. Crouse, J.L. Campbell and W.S. Hopkins, A parallelized molecular collision cross section package with optimized accuracy and efficiency. Analyst. **144**, 1660–1670 (2019). doi:10.1039/C8AN02150C
[92] L. Zanotto, G. Heerdt, P.C. Souza, G. Araujo and M.S. Skaf, High performance collision cross section calculation—HPCCS. J Comput Chem. **39**, 1675–1681 (2018). doi:10.1002/jcc.25199
[93] Z. Zhou, X. Shen, J. Tu and Z.-J. Zhu, Large-scale prediction of collision cross-section values for metabolites in ion mobility-mass spectrometry. Anal Chem. **88**, 11084–11091 (2016). doi:10.1021/acs.analchem.6b03091
[94] M.A. Baird, P. Pathak and A.A. Shvartsburg, Elemental dependence of Structurally specific isotopic shifts in high-field Ion mobility Spectra. Anal Chem. **91**, 3687–3693 (2019). doi:10.1021/acs.analchem.8b05801
[95] J.N. Dodds and E.S. Baker, Ion mobility spectrometry: fundamental concepts, instrumentation, applications, and the road ahead. J Am Soc Mass Spectr. **30**, 2185–2195 (2019). doi:10.1007/s13361-019-02288-2
[96] K. Giles, J. Ujma, J. Wildgoose, S. Pringle, K. Richardson, D. Langridge and M. Green, A cyclic ion mobility-mass spectrometry system. Anal Chem. **91**, 8564–8573 (2019). doi:10.1021/acs.analchem.9b01838
[97] E.R. Schenk, V. Mendez, J.T. Landrum, M.E. Ridgeway, M.A. Park and F. Fernandez-Lima, Direct observation of differences of carotenoid polyene chain cis/trans isomers resulting from structural topology. Anal Chem. **86**, 2019–2024 (2014). doi:10.1021/ac403153m
[98] Y. Pu, M.E. Ridgeway, R.S. Glaskin, M.A. Park, C.E. Costello and C. Lin, Separation and identification of isomeric glycans by selected accumulation-trapped ion mobility spectrometry-electron activated dissociation tandem mass spectrometry. Anal Chem. **88**, 3440–3443 (2016). doi:10.1021/acs.analchem.6b00041
[99] A.P. Bowman, R.R. Abzalimov and A.A. Shvartsburg, Broad separation of isomeric lipids by high-resolution differential ion mobility spectrometry with tandem mass spectrometry. J Am Soc Mass Spectr. **28**, 1552–1561 (2017). doi:10.1007/s13361-017-1675-2
[100] J.L. Kaszycki, A.P. Bowman and A.A. Shvartsburg, Ion mobility separation of Peptide isotopomers. J Am Soc Mass Spectr. **27**, 795–799 (2016). doi:10.1007/s13361-016-1367-3

[101] P. Pathak, M.A. Baird and A.A. Shvartsburg, Identification of Isomers by Multidimensional isotopic shifts in high-field Ion mobility Spectra. Anal Chem. **90**, 9410–9417 (2018). doi:10.1021/acs.analchem.8b02057

[102] G. Nagy, C.D. Chouinard, I.K. Attah, I.K. Webb, S.V. Garimella, Y.M. Ibrahim, E.S. Baker and R.D. Smith, Distinguishing enantiomeric amino acids with chiral cyclodextrin adducts and structures for lossless ion manipulations. Electrophoresis. **39**, 3148–3155 (2018). doi:10.1002/elps.201800294

[103] I. Dotan, W. Lindinger and D.L. Albritton, Mobilities of various mass-identified positive and negative ions in helium and argon. J Chem Phys. **64**, 4544–4547 (1976). doi:10.1063/1.432085

[104] W. Lindinger and D.L. Albritton, Mobilities of various mass-identified positive ions in helium and argon. J Chem Phys. **62**, 3517–3522 (1975). doi:10.1063/1.430988

[105] H.J. Cooper, To what extent is FAIMS beneficial in the analysis of proteins? J Am Soc Mass Spectr. **27**, 566–577 (2016). doi:10.1007/s13361-015-1326-4

[106] C. Ieritano, J. Featherstone, A. Haack, M. Guna, J.L. Campbell and W.S. Hopkins, How Hot Are Your ions in differential mobility Spectrometry? J Am Soc Mass Spectr. **31**, 582–593 (2020). doi:10.1021/jasms.9b00043

[107] L. Viehland and D. Fahey, The mobilities of NO^{-3}, NO^{-2}, NO^{+}, and Cl^{-} in N2: A measure of inelastic energy loss. J Chem Phys. **78**, 435–441 (1983). doi:10.1063/1.444522

[108] C. Bleiholder, N.R. Johnson, S. Contreras, T. Wyttenbach and M.T. Bowers, Molecular structures and ion mobility cross sections: analysis of the effects of He and N2 buffer gas. Anal Chem. **87**, 7196–7203 (2015). doi:10.1021/acs.analchem.5b01429

[109] M.N. Young and C. Bleiholder, Molecular structures and momentum transfer cross sections: the influence of the analyte charge distribution. J Am Soc Mass Spectr. **28**, 619–627 (2017). doi:10.1007/s13361-017-1605-3

[110] J.C. May and D.H. Russell, A mass-selective variable-temperature drift tube ion mobility-mass spectrometer for temperature dependent ion mobility studies. J Am Soc Mass Spectr. **22** (2011).

[111] E.R. Dickinson, E. Jurneczko, K.J. Pacholarz, D.J. Clarke, M. Reeves, K.L. Ball, T. Hupp, D. Campopiano, P.V. Nikolova and P.E. Barran, Insights into the conformations of three structurally diverse proteins: cytochrome c, p53, and MDM2, provided by variable-temperature ion mobility mass spectrometry. Anal Chem. **87**, 3231–3238 (2015). doi:10.1021/ac503720v

[112] G. Eiceman, E. Nazarov, J. Rodriguez and J. Bergloff, Positive reactant ion chemistry for analytical, high temperature ion mobility spectrometry (IMS): effects of electric field of the drift tube and moisture, temperature, and flow of the drift gas. Int. J. Ion Mobility Spectrom. **1**, 28–37 (1998). doi:10.4271/981741

[113] M. Tabrizchi, Temperature corrections for ion mobility spectrometry. Appl Spectrosc. **55**, 1653–1659 (2001). doi:10.1366/0003702011953964

[114] C.-K. Siu, Y. Guo, I.S. Saminathan, A.C. Hopkinson and K.M. Siu, Optimization of parameters used in algorithms of ion-mobility calculation for conformational analyses. J Phys Chem B. **114**, 1204–1212 (2010). doi:10.1021/jp910858z

[115] J.W. Lee, H.H.L. Lee, K.L. Davidson, M.F. Bush and H.I. Kim, Structural characterization of small molecular ions by ion mobility mass spectrometry in nitrogen drift gas: improving the accuracy of trajectory method calculations. Analyst. **143**, 1786–1796 (2018). doi:10.1039/C8AN00270C

[116] M. Waldman and R.G. Gordon, Scaled electron gas approximation for intermolecular forces. J Chem Phys. **71**, 1325–1339 (1979). doi:10.1063/1.438433

[117] L.A. Viehland, E. Mason and S. Lin, Test of the interaction potentials of H— and Br— ions with He atoms and of Cl— ions with Ar atoms. Phys Rev A. **24**, 3004 (1981). doi:10.1103/PhysRevA.24.3004

[118] A.A. Shvartsburg, S.V. Mashkevich and K.M. Siu, Incorporation of thermal rotation of drifting ions into mobility calculations: drastic effect for heavier buffer gases. J Phys Chem A. **104**, 9448–9453 (2000). doi:10.1021/jp001753a

[119] M. Fasciotti, G.B. Sanvido, V.G. Santos, P.M. Lalli, M. McCullagh, G.F. de Sá, R.J. Daroda, M.G. Peter and M.N. Eberlin, Separation of isomeric disaccharides by traveling wave ion

mobility mass spectrometry using CO_2 as drift gas. J Mass Spectrom. **47**, 1643–1647 (2012). doi:10.1002/jms.3089

[120] G.A. Bataglion, G.H.M.F. Souza, G. Heerdt, N.H. Morgon, J.D.L. Dutra, R.O. Freire, M.N. Eberlin and A. Tata, Separation of glycosidic catiomers by TWIM-MS using CO2 as a drift gas. J Mass Spectrom. **50**, 336–343 (2015). doi:10.1002/jms.3532

[121] R. Gopalakrishnan, T. Thajudeen and C.J. Hogan Jr, Collision limited reaction rates for arbitrarily shaped particles across the entire diffusive Knudsen number range. J Chem Phys. **135**, 054302 (2011). doi:10.1063/1.3617251

[122] K.J. Pacholarz, M. Porrini, R.A. Garlish, R.J. Burnley, R.J. Taylor, A.J. Henry and P.E. Barran, Dynamics of intact immunoglobulin G explored by drift-tube ion-mobility mass spectrometry and molecular modeling. Angew Chem, Int Ed. **53**, 7765–7769 (2014). doi:10.1002/anie.201402863

[123] I.D. Campuzano, C. Larriba, D. Bagal and Schnier, P.D. in *State-of-the-Art and Emerging Technologies for Therapeutic Monoclonal Antibody Characterization Volume 3. Defining the Next Generation of Analytical and Biophysical Techniques* (American Chemical Society, Washington D.C., 2015), pp. 75–112.

[124] H. Yang, Y. Drossinos and C.J. Hogan Jr, Excess thermal energy and latent heat in nanocluster collisional growth. J Chem Phys. **151**, 224304 (2019). doi:10.1063/1.5129918

[125] Tamadate, T., Higashi, H., Seto, T., Hogan, C., Calculation of the Ion-Ion Recombination Rate Coefficient via a Hybrid Continuum-Molecular Dynamics Approach. arXiv preprint arXiv:2001.03607. (2020)

[126] R. Lai, E.D. Dodds and H. Li, Molecular dynamics simulation of ion mobility in gases. J Chem Phys. **148**, 064109 (2018). doi:10.1063/1.4998955

[127] W.F. Siems, L.A. Viehland and H.H. Hill Jr, Improved momentum-transfer theory for ion mobility. 1. derivation of the fundamental equation. Anal Chem. **84**, 97829791 (2012). doi:10.1021/ac301779s

[128] Gandhi, V., Larriba-Andaluz, C., Deviations from the Mason-Schamp Equation for Small Molecules; an Ion Mobility study. Proceedings of the 68th ASMS Conference on Mass Spectrometry and Allied Topics, ThOB1010, Houston, Texas. (2020)

Appendices

Appendix A. Theoretical calculation of ion mobility and the ion collision cross section

Although the method employed in this section is not the most general method to calculate the mobility of ion in the free molecular regime, its conceptual significance should not be underestimated. The method assumes that both gas distribution and ion distribution in the gas phase are known. The result from this approach is only valid at zero fields and large ion masses but can be extrapolated to small ion masses and high fields with a minor change (see Appendix C). Let us start by assuming that we have a distribution of gas molecules of mass m which is based on the Maxwell Boltzmann distribution. The probability density function of gas molecules with velocity c_i at temperature T is given by

$$f(c_i) = \left(\frac{m}{2\pi kT}\right)^{3/2} e^{-\frac{mc^2}{2kT}}, \tag{A.1}$$

where k is the Boltzmann constant. Let us also assume that the ion is in thermal equilibrium with the gas (one-temperature theory) and that it drifts with a constant drift velocity v_{di}. The probability density function of an ion of mass M with velocity z_i will be given by

$$F(z_i) = \left(\frac{M}{2\pi kT}\right)^{3/2} e^{-\frac{M(z_i - v_{di})^2}{2kT}} = \left(\frac{M}{2\pi kT}\right)^{3/2} e^{-\frac{Mz_i^2}{2kT}} e^{+\frac{2Mz_i \cdot v_{di}}{2kT}} e^{-\frac{Mv_{di}^2}{2kT}} \tag{A.2}$$

Note that the distribution of the ions is skewed due to the appearance of the drift velocity. Without going into details about the reason for the change, a two-temperature theory description is also

possible by changing the effective temperature of the ion probability density function to $T_{eff} = T + mv_d^2/3k$.

Given the ion and gas distributions, the idea is to calculate the drag force exerted by the impinging gas molecules on the ion, which is assumed fixed at a particular orientation (although an averaging will be done over all orientations at the end). This may be done by calculating the average momentum transfer per unit time, which requires the exercise of calculating momentum exchange, final minus initial, of the ion with all gas molecules that interact with it. The exchange will depend on the relative velocity and interaction potential between each individual gas molecule and ion. Since the ion is not necessarily spherical, the interaction might vary depending on the region of impingement within the ion and gas and subsequent reemission (which could potentially be inelastic). In order to start the interaction, one may calculate the collision frequency of 'point' gas molecules into a differential of surface $d\Sigma = d_{eff}^2 \sin\psi \, d\psi \, d\epsilon$ of a singular ion as depicted in Figure A1 with the colatitude and azimuthal angles $\psi and \epsilon$ as described. Here d_{eff} is an effective distance that resembles the sphere of influence of ion and gas molecule which is not necessarily constant and may depend on potential interactions, e.g. the sum of radii for hard sphere interactions. To mathematically tackle the problem, it is a good idea to use the relative velocity g_i between gas molecule and ion which is given by

$$g_i = z_i - c_i \tag{A.3}$$

In that case, one can assume the ion to be static and the gas molecule are point particles incoming with velocity g_i onto the sphere of influence of the ion. If n_{gas} is the gas number concentration, the collision frequency of gas molecules impinging the differential of surface is given by those gas molecules contained in the cylinder with a base area $d\Sigma$ and a height corresponding to the component of the relative velocity in the direction normal to the surface. As such, the collision frequency probability of a gas molecule having velocities between c_i and $c_i + dc_i$ (with i between 1 and 3) colliding with an ion having velocities between z_i and $z_i + dz_i$ at the differential of surface $d\Sigma$ is then given by

$$n_{gas} g_i \cdot n_i|_{g_i \cdot n_i < 0} F(z_i) f(c_i) dc_1 dc_2 dc_3 dz_1 dz_2 dz_3 d_{eff}^2 \sin\psi \; d\psi \, d\epsilon \tag{A.4}$$

where n_i is the normal to the surface and $g_i \cdot n_i = g\cos\psi$. The $|_{g_i \cdot n_i < 0}$ is to emphasise that only gas molecules colliding with the outside of the surface (positive relative velocity) should be counted.

If the reemitted velocity after collision is given by c_j' (being z_j' the reemission velocity for the ion after impact), the total momentum exchange Δp_{gas_j} for every individual gas molecule can then be

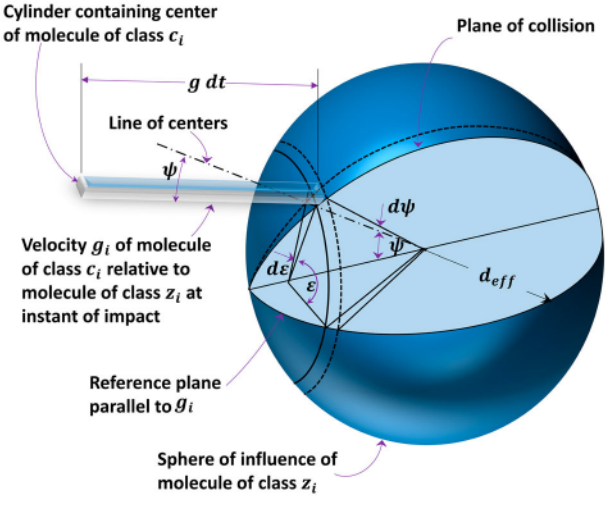

Figure A1. Reconstruction of the collision of gas molecules with a single ion. Adapted from from Vincenti and Kruger.

calculated as

$$\Delta p_{gas_j} = m(c'_j - c_j) \tag{A.5}$$

And the momentum exchange probability distribution is therefore:

$$n_{gas} m(c_j - c_j^{'}) g_i \cdot n_i|_{g_i \cdot n_i < 0} F(z_i) f(c_i) dc_1 dc_2 dc_3 dz_1 dz_2 dz_3 \sin\psi \, d\psi \, d\epsilon \tag{A.6}$$

Given the existence of 3 inter-related velocities in Equation (A.6) it is customary and normally easier to operate using the centre of mass velocity and the relative velocity as the variables of interest. The centre of mass velocity is given by

$$W_i = \frac{mc_i + Mz_i}{m + M} \tag{A.7}$$

so that:

$$c_i = W_i - \frac{M}{m+M} g_i \; and \; z_i = W_i + \frac{m}{m+M} g_i \tag{A.8}$$

The change of differentials is given by the Jacobian:

$$dc_i dz_i = \begin{vmatrix} \frac{\partial c_i}{\partial W_i} & \frac{\partial c_i}{\partial g_i} \\ \frac{\partial z_i}{\partial W_i} & \frac{\partial z_i}{\partial g_i} \end{vmatrix} dW_i dg_i = 1 \cdot dW_i dg_i \tag{A.9}$$

Upon the change of variables, one arrives at the following probability equation:

$$n_{\text{gas}} m(c_j - c_j^{'}) g_i \cdot n_i|_{g_i \cdot n_i < 0} \left(\frac{mM}{(2\pi kT)^2} \right)^{3/2} e^{-\frac{(M+m)W^2 - 2MW_i \cdot v_{di} + M^2/(m+M) v_{di}^2}{2kT}} e^{-\frac{\mu(g - v_{di})^2}{2kT}}$$
$$\times \, dg_1 dg_2 dg_3 dW_1 dW_2 dW_3 d_{eff}^2 \sin\psi d\psi d\epsilon \tag{A.10}$$

where $\mu = \frac{mM}{m+M}$ is the reduced mass. To ease the results, the variable centre of mass velocity W_i can be integrated from $-\infty$ to ∞ as long as $(c_j - c_j')$ is independent of W_i (as shown below), yielding the following new probability distribution of relative velocity:

$$n_{gas} m(c_j - c_j^{'}) g \left(\frac{\mu}{2\pi kT} \right)^{3/2} e^{-\frac{\mu(g - v_{di})^2}{2kT}} dg_1 dg_2 dg_3 d_{eff}^2 \cos\psi \, \sin\psi \, d\psi \, d\epsilon \tag{A.11}$$

Here, $g_i \cdot n_i$ has been substituted and ψ must be integrated only from 0 to $\pi/2$ to comply with the positive velocity requirement.

Since d_{eff} and the sphere of influence is not easily tractable for non-spherical ions and gas molecules, it is easier to make use of the impact parameter b (see Figure A2) to describe a differential cross section. From geometrical arguments, $b = d_{eff} \sin\psi$ and $db = d_{eff} \cos\psi \, d\psi \, d\epsilon$ and therefore:

$$d_{eff}^2 \sin\psi \, \cos\psi \, d\psi \, d\epsilon = bdbd\epsilon = dP_c \tag{A.12}$$

Substituting:

$$n_{gas} m(c_j - c_j^{'}) g \left(\frac{\mu}{2\pi kT} \right)^{3/2} e^{-\frac{\mu(g_i - v_{di})^2}{2kT}} dg_1 dg_2 dg_3 bdbd\epsilon \tag{A.13}$$

where b can have values from 0 to ∞ to account for positive relative velocities only. One would like, at this point, to refer the momentum exchange $(c_j - c_j')$ of the gas molecules to the relative velocity in order to be able to integrate the probability distribution. To do this, one can make use of the centre of mass frame. The velocities of the ion and gas molecule ($\tilde{z}_j$ and $\tilde{c}_j$) in the centre-of-mass reference frame are given by

$$\tilde{c}_j = c_j - W_j = -\frac{M}{m+M} g_j = -\frac{\mu}{m} g_j \tag{A.14}$$

$$\tilde{z}_j = z_j - W_j = \frac{m}{m+M} g_j = \frac{\mu}{M} g_j \tag{A.15}$$

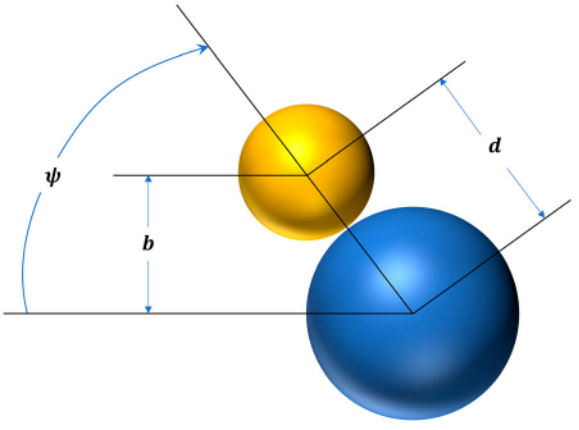

Figure A2. Transformation of azimuthal angle into impact parameter. Adapted from from Vincenti and Kruger.

On the other hand, assuming conservation of momentum upon collision:

$$m\tilde{c}_j + M\tilde{z}_j = m\tilde{c}'_j + M\tilde{z}'_j,$$

since the centre of mass is not modified upon collision. Equations (A.14) and (A.15), i.e. the momenta are equal but opposite, establishes the following equalities to be used later:

$$m\tilde{c}_j = M\tilde{z}_j \tag{A.16}$$

$$m\tilde{c}'_j = M\tilde{z}'_j \tag{A.17}$$

Moreover, assuming elastic interaction and conservative potentials, conservation of energy upon collision gives:

$$\frac{1}{2}m\tilde{c}^2 + \frac{1}{2}M\tilde{z}^2 + \frac{1}{2}(m+M)W^2 = \frac{1}{2}m\tilde{c}'^2 + \frac{1}{2}M\tilde{z}'^2 + \frac{1}{2}(m+M)W^2 \tag{A.18}$$

Substitution of the momenta equalities (Equations (A.14) and (A.15)) in the energy conservation equation yields the only possible solution for the magnitudes:

$$g = g' \text{ with } \tilde{c} = \tilde{c}' \text{ and } \tilde{z} = \tilde{z}' \text{ and thus } c = c'$$

From the point of view of the centre of mass, the velocities are parallel but opposite, both before and after the collision. This can be observed in Figure A3.

The deflection angle χ may be defined in the centre of mass coordinates (see Figure A3) as the deflection angle between impinging and reemitted trajectories and, as such, should only depend on the impact parameter b, the relative velocity and the potential between the interacting particles. Therefore $\chi = \chi(b, g, \Phi)$, being Φ the potential interaction. Using a vector parallel and perpendicular $(e_{j\parallel}, e_{j\perp})$ to the initial relative velocity g_j inside the plane formed by the line of centres k_i and by g_j, the momentum exchange can be given from geometric considerations by

$$c'_j - c_j = \tilde{c}'_j - \tilde{c}_j = \frac{M}{m+M}\left(2g_j \sin^2\left(\frac{\chi}{2}\right) + g\ \sin(\chi)\, e_{j\perp}\right) \tag{A.19}$$

Since $2\sin^2\left(\frac{\chi}{2}\right) = 1 - \cos(\chi)$ then:

$$m(c'_j - c_j) = \mu g_j(1 - \cos(\chi)) + \mu g \sin(\chi) e_{j\perp} \tag{A.20}$$

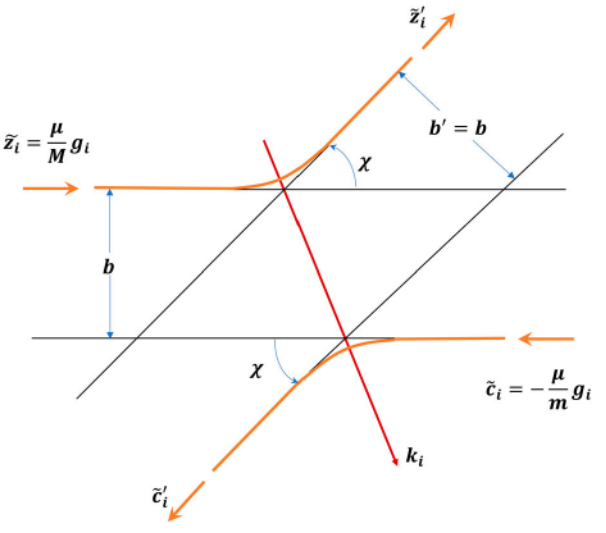

Figure A3. Centre of mass representation of the molecular trajectories during a collision. Adapted from from Vincenti and Kruger.

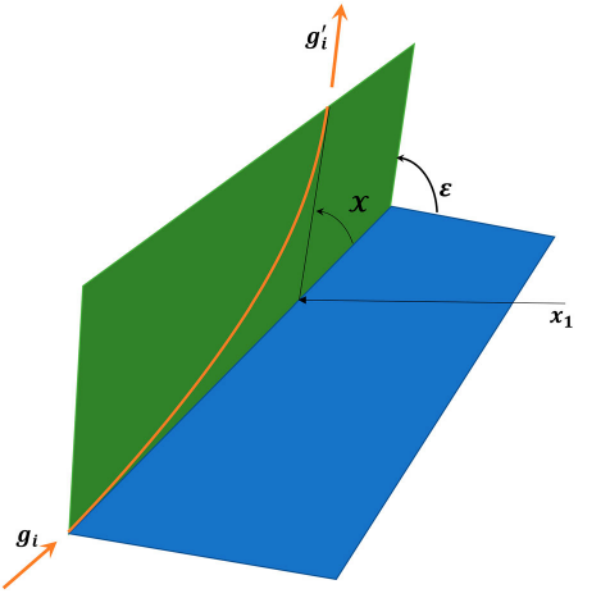

Figure A4. Defining the deflection trajectory in 3D with respect to the centre of mass. Adapted from from Vincenti and Kruger.

Using the ϵ angle to describe the out of plane angle (see Figure A4), the cartesian coordinates of $e_{j\perp}$ are given by

$$e_{1\perp} = \sqrt{1 - g_1/g^2}\cos\epsilon\,\vec{i} \tag{A.21}$$

$$e_{2\perp} = -\left(\frac{g_2 g_1 \cos\epsilon + g g_3 \sin\epsilon}{g\sqrt{g^2 - g_1^2}}\right)\vec{j} \tag{A.22}$$

$$e_{3\perp} = -\left(\frac{g_3 g_1 \cos\epsilon + g g_2 \sin\epsilon}{g\sqrt{g^2 - g_1^2}}\right)\vec{k} \tag{A.23}$$

When equation (A.20) is introduced into our probability distribution, the second term on the right-hand side, $2\mu g e_{j_\perp}$, will disappear after sampling over all possible ϵ angles from 0 to 2π. What is left can be regarded as the momentum exchange of a gas molecule (may also be regarded as a quantity of persistence in the direction of relative velocity) with the ion. Bringing the first term into our probability distribution and integrating over ϵ:

$$n_{gas}\mu g g_j\left(\frac{\mu}{2\pi kT}\right)^{3/2} e^{-\frac{\mu(g_i - v_{di})^2}{2kT}} dg_1 dg_2 dg_3 2\pi b(1 - \cos(\chi))db \tag{A.24}$$

The next step is to transform the cartesian coordinates into spherical coordinates as

$$dg_1 dg_2 dg_3 = g^2 \sin\theta_g \, dg d\theta_g d\phi_g \tag{A.25}$$

where θ_g and ϕ_g are the azimuthal and colatitude angles. The g_j vector can be written in the spherical coordinates as $g_j = g(\cos\theta_g, \sin\theta_g\cos\phi_g, \sin\theta_g\sin\phi_g)$. By doing so, one arrives at the expression:

$$n_{gas}\mu g^4(\cos\theta_g \sin\theta_g, \sin\theta_g^2 \cos\phi_g, \sin\theta_g^2 \sin\phi_g)\left(\frac{\mu}{2\pi kT}\right)^{3/2} e^{-\frac{\mu(g_i - v_{di})^2}{2kT}} dg d\theta_g d\phi_g 2\pi b(1 - \cos(\chi))db \tag{A.26}$$

One can integrate the angular components θ_g from 0 to π and ϕ_g from 0 to 2π. The problem here however relies on the fact that the exponential still has to be transformed into spherical coordinates and integrated which is not a simple task analytically. One can resort to linearising the exponential in the equation prior to its integration. The assumption generally employed is that of small drift velocities (small Mach numbers) where it is assumed that $v_d \ll g$. This assumption is equivalent to the linearisation employed by Chapman and Enskog to solve the Boltzmann equation. The exponential can then be written as

$$e^{-\frac{\mu(g_i - v_{di})^2}{2kT}} = e^{-\frac{\mu g^2}{2kT}} e^{-\frac{\mu v_d^2}{2kT}} e^{\frac{2g_i v_{di}}{2kT}} \sim e^{-\frac{\mu g^2}{2kT}} e^{\frac{2g_i v_{di}}{2kT}} = e^{-\frac{\mu g^2}{2kT}}\left(1 + 2\frac{\mu}{2kT} g_i v_{d_i} + \cdots\right) \tag{A.27}$$

where the relation $e^x = \sum_{n=0}^{n=\infty} x^n/n!$ has been used to expand the last term of the second and third equalities and $v_d^2 \ll g^2$ is considered negligible. To make the calculation slightly easier, one can assume that the drift velocity is in the x direction $v_{d_i} = (v_d, 0, 0)$ and $g_i v_{di} = (g_1 v_d + 0 + 0) = (g\cos\theta_g v_d)$:

$$n_{gas}\mu g^4(\cos\theta_g \sin\theta_g, \sin\theta_g^2 \cos\phi_g, \sin\theta_g^2 \sin\phi_g)\left(\frac{\mu}{2\pi kT}\right)^{3/2} e^{-\frac{\mu g^2}{2kT}}\left(1 + 2\frac{\mu}{2kT} g \cos\theta_g v_d + \cdots\right)$$
$$\times \, dg d\theta_g d\phi_g 2\pi b(1 - \cos(\chi))db \tag{A.28}$$

Now, in the expansion in brackets, $\left(1 + 2\frac{\mu}{2kT} g_i v_{d_i} + \cdots\right)$, the first term by itself corresponds to the case where no drift velocity exists. As such, when trying to integrate over all possibilities, the momentum exchange would be 0 on average.

A pause has to be made at this particular point to discuss the meaning of Equation (28) in terms of the direction of the drag force with respect to the direction of the drift velocity. Under a non-spherical ion, it could be expected that the direction of the drag force (namely the result of Equation (A.28)) does not necessarily have to be in the direction of the drift. This suggests that the mobility can be regarded as a second-order tensor so that:

$$qE_i = F_{Di} = B_{ij} v_{d_j} \tag{A.29}$$

The prediction of the symmetric B_{ij} tensor would require that the calculation of the drag force is done in 3 perpendicular orientations of the ion which may be averaged afterwards. This may be simplified as long as all orientations are equally probable, which then suggests that when averaging only the resultant force in the direction of the field will be non-zero and that drift velocity and field

will be aligned (on average):

$$q\langle E_i\rangle = q\mathrm{E} = \langle B_{ij}\rangle\langle v_{dj}\rangle = F_f v_d \tag{A.30}$$

Under this assumption of equal probability of orientations, the momentum transfer per unit time (drag force) is in the direction of the drift velocity (x direction in this case), and the equation reduces to:

$$n_{gas}\mu g^5\left(\frac{\mu}{2\pi kT}\right)^{3/2} e^{-\frac{\mu g^2}{2kT}}\left(\frac{\mu}{kT}v_d + \cdots\right) dg\cos^2\theta_g \sin\theta_g\, d\theta_g d\phi_g 2\pi b(1-\cos(\chi))db \tag{A.31}$$

One can now integrate the relative velocity angles θ_g *and* ϕ_g. This integration yields:

$$\frac{4\pi}{3} n_{gas}\mu\left(\frac{\mu}{2\pi kT}\right)^{3/2} g^5 e^{-\frac{\mu g^2}{2kT}}\left(\frac{\mu}{kT}v_d + \cdots\right) dg 2\pi b(1-\cos(\chi))db \tag{A.32}$$

To simplify the picture, a change of variable may be done using the most probable speed:

$$g^* = \frac{g}{h}\,;\; h = \sqrt{\frac{2kT}{\mu}} \tag{A.33}$$

With this change in mind and removing higher-order terms of the expansion:

$$\frac{8}{3\pi} n_{gas} v_d \sqrt{2kT\pi\mu} g^{*5} e^{-g^{*2}} dg^* 2\pi b(1-\cos(\chi))db \tag{A.34}$$

To get the total drag force of all gas molecules, one can integrate over all possible values of g^* from 0 *to* ∞ and all possible values of b from 0 *to* ∞.

$$F_{D_i} = \frac{8}{3\pi} n_{gas} v_{d_i}\sqrt{2kT\pi\mu}\int_0^\infty g^{*5} e^{-g^{*2}} dg^* \int_0^\infty 2\pi b(1-\cos(\chi))db \tag{A.35}$$

For the result in Equation (A.35) to be correct, the underlying assumption is that all orientations are equally correct. Using the Euler angles θ, ϕ, γ for the orientation of the ion, one can integrate over all angles:

$$\bar{F}_{D_i} = F_f v_{d_i} = \frac{8}{3\pi} n_{gas} v_{d_i}\sqrt{2kT\pi\mu}\frac{1}{8\pi^2}\int_0^{2\pi}\int_0^{\pi} sin\phi \int_0^{2\pi}\int_0^\infty g^{*5} e^{-g^{*2}} dg^* \times \int_0^\infty 2\pi b(1-\cos(\chi))dbd\theta d\phi d\gamma \tag{A.36}$$

When the orientations are introduced, the deflection angle gains a new dependency on the orientation of the molecule. As such: $\chi = \chi(b, g, \Phi, \theta, \phi, \gamma)$. Here, the first approximation to the CCS can be defined as

$$\bar{\Omega}(1,1) = \frac{1}{8\pi^2}\int_0^{2\pi}\int_0^{\pi} sin\phi \int_0^{2\pi}\int_0^\infty g^{*5} e^{-g^{*2}} dg^* \int_0^\infty 2\pi b(1-\cos(\chi))dbd\theta d\phi d\gamma \tag{A.37}$$

From eq A.30, the mobility at low drift velocities may be calculated as

$$\langle K\rangle = \frac{q}{F_f} = \frac{ze}{F_f}, \tag{A.38}$$

where q is the charge, e is elementary charge and z is the charge number quantity. When using A.36-38, one finally arrives at (dropping the gas subindex for the number concentration):

$$\langle K\rangle = \frac{3ze}{16n}\sqrt{\frac{2\pi}{kT\mu}}\frac{1}{\bar{\Omega}(1,1)} = \frac{3ze}{16n}\left(\frac{1}{m}+\frac{1}{M}\right)^{\frac{1}{2}}\sqrt{\frac{2\pi}{kT}}\frac{1}{\bar{\Omega}(1,1)} \tag{A.39}$$

This result agrees with the results from Kihara's first approximation from the one-temperature theory. As will be proven in Appendix B, this expression is only valid for large ion masses. However, as mentioned previously, a small change by assuming an effective temperature, extends the result of Equation (A.39) to all masses and high fields with reasonable accuracy.

Calculation of the deflection angle χ for a central force interaction

Although not required for most numerical methods, we consider here a proof for Equation (4) of the main text which relates the deflection angle χ to a central interaction potential between gas molecule an ion. This study assumes a two-body problem and the derivation is done from the point of view of conservation of energy (although it can also be done directly from momentum equations). Imagine the interaction sketched in Figure A5 where a pair of interacting particles are viewed from a reference fixed on one of the particles. The main goal is to calculate χ as a function of the potential interaction or central force of the dual particle system. The conservation of energy in the centre of mass frame of the system is given by the potential energy plus the kinetic energy with respect to a reference far away:

$$E_k = \frac{\mu}{2}[\dot{R}^2 + R^2\dot{\psi}^2] + \Phi(R) = \frac{\mu}{2}g^2 \tag{A.40}$$

Noting that the angular momentum must be conserved ($R\boldsymbol{u}_r \times R\dot{\psi}\boldsymbol{u}_\psi = R^2\dot{\psi} = \text{constant}$), it is easy to refer it to the initial angular momentum: bg. Thus, the equation above can be rewritten as

$$\frac{\dot{R}^2}{g^2} = 1 - \frac{b^2}{R^2} - \frac{\Phi(R)}{\mu g^2/2} \tag{A.41}$$

Given that $\dot{R} = \frac{dR}{d\psi}\frac{d\psi}{dt} = \frac{dR}{d\psi}\frac{bg}{R^2}$, one gets:

$$\left(\frac{dR}{d\psi}\right)^2 = \frac{R^4}{b^2}\left\{1 - \frac{b^2}{R^2} - \frac{\Phi(R)}{\frac{\mu g^2}{2}}\right\} \tag{A.42}$$

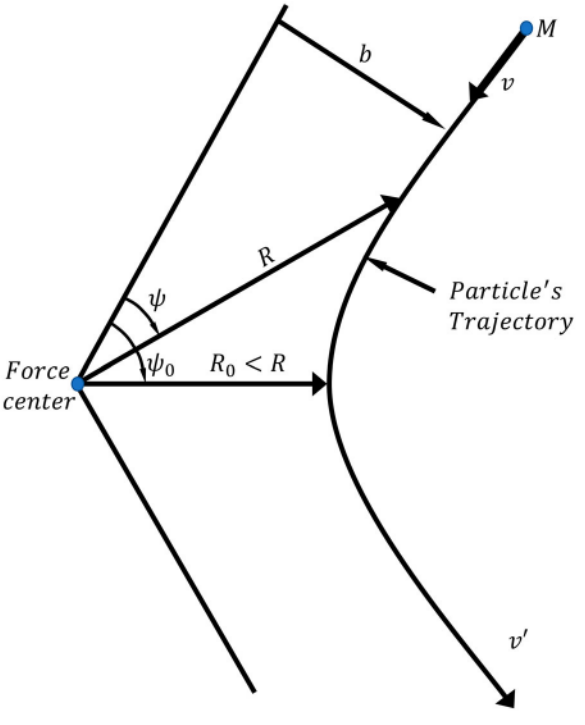

Figure A5. Centre of frame view of two particles with a central force.

Table A.1. Variables used.

Variable	Significance
$f(c_i)$	Gas velocity distribution
$F(z_i)$	Ion velocity distribution
c_i	Gas velocity
z_i	Ion velocity
m	Mass of the gas
M	Mass of the ion
k	Boltzmann's constant
T	Gas buffer temperature
v_d	Drift velocity
T_{eff}	Effective temperature
g_i	Relative velocity
$n; n_{gas}$	Gas number density
n_i	Normal to surface
Σ	Surface area
ψ	Colatitude angle
ϵ	Azimuthal angle
W_i	Centre of mass velocity
μ	Reduced mass
d_{eff}	Effective diameter
b	Impact parameter
Δp	Momentum exchange
dP_c	Collision area differential
c_i', z_i', g_i'	Velocities after reemission
$\tilde{c}_i, \tilde{z}_i$	Relative velocities with respect to centre of mass velocity
χ	Deflection angle
E_i	Electric field
q	Electric charge
z	Electric charge number/velocity magnitude
e	Elemental charge
F_{D_i}	Drag force
B_{ij}	Drag tensor
F_f	Friction factor
θ_g, ϕ_g	Relative velocity angles in spherical coordinates
h	Most probable speed
$\bar{\Omega}_T(1,1)$	Averaged first collision cross section in units of area
θ, ϕ, γ	Euler angles of orientation
$\dot{\psi}$	Angular velocity
Φ	Potential interaction
E_k	Kinetic Energy of the ion/gas pair
R	Distance from force centre
a_j	Acceleration of z_l ion velocities
$\mathcal{J}$	Lorentzian operator
$\psi_l^{(r)}$	Burnett basis functions
P_l	Lagrange polynomials
w	Velocity of the ion in the direction of the field
$S_j^{(r)}$	Sonine polynomials
$Q^{(l)}$	Collision operator
$\lambda^{(r)}$	Eigenvalues of Lorentzian operator for the Maxwell Model
$a_{rs}(l)$	Matrix elements of the Lorentzian operator linearisation
$\mathcal{E}$	Field over density dimensionless number
K	Ion mobility
K_0	Reduced ion mobility
α_i	One-temperature theory coefficients
$\Omega^{(l)}(n)$	Collision cross section flux
$\Omega(l,n)$	Collision integrals
T_b	Ion temperature two-temperature theory
$a_{rs}^*(l)$	Matrix coefficients for two-temperature theory

(*continued*)

Table A.1. Continued.

Variable	Significance
e_μ, d, f	Mass dependent functions
K_{2T}	Two-temp approximation mobility
$\Omega^*(1,1); \bar{\Omega}^*_{T_{eff}}(1,1)$	First collision integral for two-temperature theory
α^*, β^*	Two-temperature theory higher approximation coefficient

Which can be solved between infinity and the apsidal distance (R_0, ψ_0):

$$\psi_0 = \int_0^{\psi_0} d\psi = \int_\infty^{R_0} \frac{bdR}{R^2\left[1 - \frac{b^2}{R^2} - \frac{\Phi(R)}{\frac{\mu g^2}{2}}\right]} \tag{A.43}$$

Note that the relation between ψ and χ is: $\chi = \pi - 2\psi_0$, hence:

$$\chi = \pi - 2\int_\infty^{R_0} \frac{bdR}{R^2\left[1 - \frac{b^2}{R^2} - \frac{\Phi(R)}{\frac{\mu g^2}{2}}\right]} \tag{A.44}$$

The apsidal distance R_0 (effective diameter for a collision) can be calculated using equation (A.41). Rearranging the equation and noting that $\dot{R} = 0$ at the apsidal point R_0:

$$R_0^2 = b^2 / \left[1 - \frac{2\Phi(R_0)}{g^2\mu}\right] \tag{A.45}$$

The effective diameter d_{eff} can also be inferred for two hard spheres with an attractive potential. If the apsidal distance R_0 for given arm b, coincides with the sum of the radii of ion and gas molecule: $d = r_{ion} + r_{gas}$, then the effective diameter that will result in a collision will be given by the arm. Thus:

$$\mathrm{d}^2_{eff,s} = d^2\left[1 - \frac{2\Phi(d)}{g^2\mu}\right] \tag{A.46}$$

Appendix B. Kihara's approximation to mobility from Mason and Schamp's point of view

To understand Kihara's approximation to ion mobility at high fields, it is indispensable that we describe the ion distribution by using the solution to the Boltzmann equation for an ion in a buffer gas. This is in contrast to our approach in Appendix A, where a distribution is already assumed for ions of a known drift velocity. It turns out, however, that the distribution in Appendix A is only valid for vanishing fields and a more general theory must be employed if one were to study the effect of high fields. As such, the Boltzmann equation for an ion distribution $F(z_i)$ in a bath of gas is given by (See Table A.I.):

$$\frac{\partial F}{\partial t} + z_j\frac{\partial F}{\partial x_j} + a_j\frac{\partial F}{\partial z_j} = \frac{DF}{Dt} = n\int\int\int (f'F' - fF)gbdbd\epsilon dc_i, \tag{B.1}$$

where $dc_i = dc_1 dc_2 dc_3$ corresponds to all gas molecule velocities between c_i and dc_i. To come up with equation B.1, several simplifications have already been made. The most important one is to assume that the number density N of ions is much smaller than the density of gas molecules n. It is indeed small enough that we can neglect collisions of ions with other ions. Under such circumstances, the only collision term appearing on the right-hand side is that of collisions of the ion with the gas of distribution of $f(c_i)$, where the distribution $f(c_i)$ for the gas is assumed to be Maxwellian as portrayed by Equation (A.1). In the collision term, prime distributions correspond to those of molecules and ions of velocities c_i' and z_i' which replenish velocities of class z_i after a collision. If we assume that our distribution $F(z_i)$ does not depend on position and that a steady state for our process has been reached (a reasonable assumption in a drift tube for example), the first two terms on the left-hand side can be dropped and the equation becomes:

$$\frac{qE_j}{Mn}\frac{\partial F}{\partial z_j} = \frac{eE}{Mn}\frac{\partial F}{\partial w} = \int\int\int (f'F' - fF) g b db d\epsilon dc_i \tag{B.2}$$

where the only non-negligible acceleration present for the ions of mass M and single charge e is that of the electric field. In particular, if the field is constant in a known axis direction, the left-hand side has only one term where w is now the velocity that axis direction (e.g. $z_1 = w$). Even under the current simplified version, Equation (B.2) is by no means simple to solve. In fact, there is only a handful of solutions for very specific approximations. Our single hope is to resort to solving moments of the distribution. That is, multiply the above equation by a function of the ion's velocity and integrate over all z_i velocities producing an equation that is averaged but possible to solve and which yields a piece of information about the distribution, e.g. the average drift velocity, the ion energy ... which more often than not would be the information one would seek if the full distribution was known.

Before we proceed with the moments of the equation, it is beneficial to write the right-hand side in terms of an operator, $\mathcal{J}$, known as the Lorentz or Boltzmann operator. To do so, we can assume without loss of generality that the ion population can be described in terms of $F^{(0)}$, the Maxwellian equilibrium distribution in the absence of a field, as

$$F = F^{(0)}(1+\Phi) = \left(\frac{M}{2\pi kT}\right)^{\frac{3}{2}} e^{-\frac{M(z_i)^2}{2kT}}(1+\Phi) \tag{B.3}$$

so that Equation (B.2) becomes ($\mathcal{J}(1) = 0$):

$$\frac{eE}{Mn}\frac{\partial F}{\partial w} = -F^{(0)}\mathcal{J}\Phi \tag{B.2'}$$

where the linear operator $\mathcal{J}$ for any particular function $\alpha(z_i)$ of the velocity is given by

$$\mathcal{J}\alpha = \int\int\int f(\alpha - \alpha') g b db d\epsilon dc_i \tag{B.4}$$

and where the dependence on z_i of α has been removed for brevity. Ideally, one would like to find ways to solve the moments of Equation (B.2'). A moment that is particularly useful is that of the velocity w in the direction of the field which can be related to the drift velocity and to the mobility of the ion. In general, to obtain a moment equation, all that needs to be done is to multiply Equation (B.2') by a function that depends on the ion velocity $\alpha(z_i)$ and integrate overall possible velocities. This yields:

$$\frac{eE}{Mn}\int \frac{\partial F}{\partial w}\alpha dz_i = -\int F^{(0)}\alpha\mathcal{J}\Phi dz_i \tag{B.5}$$

Let's define at this point the inner product of two functions as

$$(\phi, \psi) = \int F^{(0)}\phi\psi dz_i \tag{B.6}$$

Let's assume that the linear operator $\mathcal{J}$ is symmetric under this inner product $(\phi, \mathcal{J}\psi) = (\mathcal{J}\phi, \psi)$. While this symmetry was proven to be unnecessary to arrive at the same final equation

as shown by Viehland and Mason, it is used here for the purpose of simplicity. Using integration by parts on the left and the symmetry property on the right, one arrives at:

$$\frac{eE}{Mn}\int F\frac{\partial\alpha}{\partial w}dz_i = \int F\mathcal{J}\alpha dz_i \tag{B.7}$$

Both sides of the equation in B.7 represent average quantities (moments) of the equation. Therefore:

$$\frac{eE}{Mn}\left(\frac{\partial\alpha}{\partial w}\right)_{Av} = \langle\mathcal{J}\alpha\rangle_{Av} \tag{B.8}$$

In the particular case of $\alpha = w$, the velocity in the direction of the field, equation B.8 becomes:

$$\frac{eE}{Mn} = \langle\mathcal{J}w\rangle_{Av}, \tag{B.9}$$

where the only thing left to do is to calculate the average of the $\mathcal{J}$ operator in order to obtain an approximation for the mobility, a task that is by no means arithmetically simple. Equation (B.9) should be reminiscent of the Equation (A.6) as it relates the electrical force to a quantity that must be related to the drag force of the ion (momentum transfer per unit time).

A general approach to solve Equation (B.8) is to find suitable α expressions that may be available to solve the $\mathcal{J}$ operator in an effortless manner. This is usually obtained by choosing α to be a complete set of functions. The most suitable functions presented to date, referred to as modified Burnett functions, are generally specified as

$$\psi_l^{(r)} = \left(\frac{Mz^2}{2kT}\right)^{\frac{l}{2}} P_l\left(\frac{w}{z}\right) S_{l+\frac{1}{2}}^{(r)}\left(\frac{Mz^2}{2kT}\right) \tag{B.10}$$

Here P_l are the Legendre polynomials, while $S_j^{(r)}$ are the Sonine (associated Laguerre) polynomials. The reason these functions are chosen is that they correspond to eigenfunctions of the $\mathcal{J}$ operator in the Maxwellian model r^{-4}, that is, when the collisional operator $Q^{(l)} = \int^2 \pi(1 - cos^l(\chi))bdb$ is independent of the relative velocity g. Under such situation:

$$\mathcal{J}_{Maxwell}\psi_l^{(r)} = \lambda_l^{(r)}\psi_l^{(r)} \tag{B.11}$$

The importance of the result from Equation (B.11) should not be underestimated. It suggests that the basis functions in Equation (B.10) are eigenfunctions of the operator $\mathcal{J}_{Maxwell}$ and hence the $\lambda_l^{(r)}$ are the eigenvalues. While the Maxwellian model will not hold true for real ions, it is true that under most circumstances the r^{-4} attraction term is the most important long-range potential which suggests that the solution to a more general potential should be a perturbation to the result presented in Equation (B.11). At this point, it would be possible to calculate the $\lambda_l^{(r)}$ eigenvalues and provide a solution to Equations (B.8)–(B.9). However, the estimations of $\lambda_l^{(r)}$ values are simplified versions of more complex calculations performed below and will not be pursued here. For completeness, Table B.I provides some of the most common eigenfunctions $\psi_l^{(r)}$ and eigenvalues $\lambda_l^{(r)}$.

For a more general theory of mobility, one can assume instead that the solution to the operator is a series of the Burnett functions that includes off-diagonal terms. That is:

$$\mathcal{J}\psi_l^{(r)} = \sum_s a_{rs}(l)\psi_l^{(s)}, \tag{B.12}$$

where the $a_{rs}(l)$ coefficients can be calculated making use of the orthogonal inner product presented above in Equation (B.6) as

$$a_{rs}(l) = (\psi_l^{(s)}, \mathcal{J}\psi_l^{(r)})/(\psi_l^{(s)}, \psi_l^{(s)}) \tag{B.13}$$

Using algebraic relations of Legendre and Sonine polynomials:

$$\frac{d}{dx}S_m^{(n)}(x) = -S_{m+1}^{(n-1)}(x); \frac{x^2-1}{n}\frac{d}{dx}P_n(x) = xP_n(x) - P_{n-1}(x)$$

$mS_m^{(n)}(x) - xS_{m+1}^{(n-1)}(x) = (m+n)S_{m-1}^{(n)}(x)\,;\ (2n+1)xP_n(x) - (n+1)P_{n+1}(x) = -nP_{n-1}(x)$
leads to:

$$\left(l+\frac{1}{2}\right)\frac{eE}{Mn}\left(\frac{2kT}{M}\right)^{\frac{1}{2}}\frac{\partial\psi_l^{(r)}}{\partial w} = l\left(l+\frac{1}{2}+r\right)\psi_{l-1}^{(r)} - (l+1)\psi_{l+1}^{(r-1)}, \tag{B.14}$$

where when using Equation (B.9), one can establish a relation between different eigenfunctions and the operator:

$$\left(l+\frac{1}{2}\right)\langle\mathcal{J}\psi_l^{(r)}\rangle_{Av} = \mathcal{E}\left[l\left(l+\frac{1}{2}+r\right)\langle\psi_{l-1}^{(r)}\rangle_{Av} - (l+1)\langle\psi_{l+1}^{(r-1)}\rangle_{Av}\right] \tag{B.15}$$

And where:

$$\mathcal{E} = \left(\frac{eE}{Mn}\right)\left(\frac{M}{2kT}\right)^{1/2} \tag{B.16}$$

Equation (B.15) is also extremely useful and will be used to provide successive approximations to ion mobility. To start, let one introduce Equation (B.12) into Equation (B.15) to get:

$$\left(l+\frac{1}{2}\right)\sum_s a_{rs}(l)\langle\psi_l^{(s)}\rangle_{Av} = \mathcal{E}\left[l\left(l+\frac{1}{2}+r\right)\langle\psi_{l-1}^{(r)}\rangle_{Av} - (l+1)\langle\psi_{l+1}^{(r-1)}\rangle_{Av}\right];\{\psi_{l+1}^{(-1)}=0\} \tag{B.17}$$

Given that the Maxwellian model assumes elastic reemission for an ion-induced dipole potential $(4-\infty)$, which is generally the strongest long-range potential, one can assume that a first approximation is to assume that the off-diagonal terms are negligible (similar to obtaining eigenvalues). As such,

$$\left(l+\frac{1}{2}\right)a_{rr}(l)\langle\psi_l^{(r)}\rangle_{AvI} = \mathcal{E}\left[l\left(l+\frac{1}{2}+r\right)\langle\psi_{l-1}^{(r)}\rangle_{AvI} - (l+1)\langle\psi_{l+1}^{(r-1)}\rangle_{AvI}\right] \tag{B.18}$$

And, in particular, for $\psi_1^{(0)} = \left(\frac{M}{2kT}\right)^{1/2}w$, the above equation yields (omitting *Av*):

$$a_{00}(1)\langle\psi_1^{(0)}\rangle_I = \mathcal{E} \tag{B.19}$$

Or since $\langle w\rangle_I = v_d$:

$$\langle K\rangle_I = \frac{e}{Mn}\frac{1}{a_{00}(1)}, \tag{B.20}$$

where only $a_{00}(1) = (\psi_1^{(0)}, \mathcal{J}\psi_1^{(0)})/(\psi_1^{(0)}, \psi_1^{(0)})$ is left to calculate. The expression in Equation (B.20) will be equivalent to that calculated in Appendix A once $a_{00}(1)$ is calculated. Other moments can also be calculated. For example (to be used later in higher-order expressions) $\psi_1^{(1)}$:

$$\langle\psi_1^{(1)}\rangle_I = \frac{2}{3}\frac{\mathcal{E}}{a_{00}(1)}\left[\frac{5}{2}\langle\psi_0^{(1)}\rangle_I - 2\langle\psi_2^{(0)}\rangle_I\right] = -\frac{2}{3}\left(\frac{\mathcal{E}}{a_{00}(1)}\right)^3\left[\frac{5a_{00}(1)}{a_{11}(0)} + \frac{4a_{00}(1)}{a_{00}(2)}\right] \tag{B.21a-c}$$

$$\langle\psi_0^{(1)}\rangle_I = -\frac{2\mathcal{E}}{a_{11}(0)}\langle\psi_1^{(0)}\rangle_I = -\frac{2\mathcal{E}^2}{a_{11}(0)a_{00}(1)}$$

$$\langle\psi_2^{(0)}\rangle_I = \frac{2\mathcal{E}}{a_{00}(2)}\langle\psi_1^{(0)}\rangle_I = \frac{2\mathcal{E}^2}{a_{00}(2)a_{00}(1)}$$

Although complicated due to the operator, the result is a quadrature that can be tediously solved. Before a calculation is attempted, let us calculate higher approximations. To calculate them, off-diagonal terms must be considered in Equation (B.17). Given the difficulty of solving the general expression, one can make use of previous approximations to provide successive ones. There are different ways to do this. In here, we take the method proposed by Mason and Schamp and not that of Kihara although their solutions are equivalent. The equation for the nth approximation may be given by

$$\left(l+\frac{1}{2}\right)a_{rr}(l)\langle\psi_l^{(r)}\rangle_n = \mathcal{E}\left[l\left(l+\frac{1}{2}+r\right)\langle\psi_{l-1}^{(r)}\rangle_{n-1} - (l+1)\langle\psi_{l+1}^{(r-1)}\rangle_{n-1}\right]$$

$$-\left(l+\frac{1}{2}\right)\sum_{s=0}^{\infty}(1-\delta_{rs})a_{rs}(l)\langle\psi_l^{(r)}\rangle_{n-1} \tag{B.22}$$

where Mason and Schamp also terminate the summation at $s = n + r - 1$ instead of ∞ to keep a consistent addition of subsequent square terms for each new approximation. The associated error of neglected terms can be calculated. By repeated application of Equation (B.22), one can obtain higher approximations to the mobility. For example, for the third approximation, one can write:

$$\langle K\rangle_{III} = \langle K\rangle_I[\alpha_0 + \alpha_1\left(\frac{\mathcal{E}}{a_{00}(1)}\right)^2 + \alpha_2\left(\frac{\mathcal{E}}{a_{00}(1)}\right)^4 + \cdots] \tag{B.23}$$

Here, each α_n is a function that depends on different values of $a_{rs}(l)$. The different terms (in a format that each successive approximation is easy to remember) can be calculated and are given by

$$\alpha_0 = 1 + \frac{a_{01}(1)}{a_{00}(1)}\frac{a_{10}(1)}{a_{11}(1)} + \frac{a_{02}(1)}{a_{00}(1)}\frac{a_{20}(1)}{a_{22}(1)} + \cdots$$

$$\alpha_1 = \Psi_1^{(1)}\left[-\frac{a_{01}(1)}{a_{00}(1)} + \frac{a_{02}(1)}{a_{00}(1)}\frac{a_{21}(1)}{a_{22}(1)} + \cdots\right]$$

$$\alpha_2 = \Psi_1^{(2)}\left[-\frac{a_{02}(1)}{a_{00}(1)} + \frac{a_{01}(1)}{a_{00}(1)}\frac{a_{12}(1)}{a_{11}(1)} + \cdots\right] \tag{B.24-26}$$

Where $\Psi_1^{(n)}$ are closed dimensionless expressions (Equations (B.21a–c) have been used on B.27):

$$\Psi_1^{(1)} = \langle\psi_1^{(1)}\rangle_I\left(\frac{a_{00}(1)}{\mathcal{E}}\right)^3 = -\frac{2}{3}\frac{a_{00}(1)}{a_{11}(1)}\left[\frac{5a_{00}(1)}{a_{11}(0)} + \frac{4a_{00}(1)}{a_{00}(2)}\right] \tag{B.27}$$

$$\Psi_1^{(2)} = \langle\psi_1^{(2)}\rangle_I\left(\frac{a_{00}(1)}{\mathcal{E}}\right)^5 = -\Psi_1^{(1)}\frac{2}{3}\frac{a_{00}(1)}{a_{22}(1)}\left[\frac{7a_{00}(1)}{a_{22}(0)} + \frac{4a_{00}(1)}{5a_{11}(2)}\right] \tag{B.28}$$

At this point, two things must be pointed out. The first is the series shows the dependence of mobility on even powers of the field. Moreover, in the way Equation (B.23) is written, each new approximation adds a new higher power of the field to the expression. The second is that even for vanishing fields, $\mathcal{E} \cong 0$, Equation (B.23) is not equivalent to Equation (B.20) but carries higher-order terms. These terms, when studied, become of increasing importance as the mass of the ion becomes of the order or smaller than the mass of the gas (e.g. electrons).

In order to proceed, it is now necessary to transform the $a_{rs}(l)$ into quadratures that require only of the knowledge of the ion-neutral potential to be calculated; also known as collision integrals. To do so, one can make use of the B.13 expression starting with the inner product of the denominator. Using knowledge from the relations of the polynomials, the orthogonal inner product is given by

$$(\psi_l^{(r)}, \psi_m^{(s)}) = \int F^{(0)}\psi_l^{(r)}\psi_m^{(s)}dz_i = \frac{2}{2l+1}\frac{1}{\pi^{1/2}}\frac{1}{r!}\Gamma(l+r+3/2)\delta_{lm}\delta_{sr} \tag{B.29}$$

The numerator includes the $\mathcal{J}$ operator which complicates things. While there are some general formulas to do the calculation, here the calculation is performed for a couple different $a_{rs}(l)$ values to understand the logic behind it and to compare our results with those from Appendix A. Initially $a_{00}(1)$ will be calculated to get the first expression for mobility, followed by $a_{11}(0)$ which will be shown to give the first approximation to the ion's energy. Other values can be calculated similarly and have been tabulated in Table B.II. For $a_{00}(1)$, $(\psi_1^{(0)}, \psi_1^{(0)}) = 1/2$, and assuming $z_1 = w$, the equation becomes:

$$a_{00}(1) = 2(\psi_1^{(0)}, \mathcal{J}\psi_1^{(0)}) = 2\frac{M}{2kT}\int\int\int\int F^{(0)}fw(w-w')gbdbd\epsilon dz_i dc_i \tag{B.30}$$

With the proper changes of variables to relative velocities g and centre of mass velocity W (revisit Appendix A for full description of some of these equations):

$$z_i = W_i + \frac{m}{m+M}g_i; c_i = W_i - \frac{M}{m+M}g_i; g_i = z_i - c_i$$

$$dz_i dc_i = dW_i dg_i$$

$$(w - w') = (z_1 - z_1^{'}) = \frac{m}{m+M}(g_1 - g_1^{'}) = \frac{m}{m+M}g_1(1 - \cos(\chi))$$

$$F^{(0)}f = \pi^{-3}\left(\frac{m}{2kT}\right)^{3/2}\left(\frac{M}{2kT}\right)^{3/2} e^{-\frac{m+M}{2kT}W^2} e^{-\frac{\mu}{2kT}g^2},$$

one can write:

$$a_{00}(1) = 2\frac{\mu}{2kT}\pi^{-3}\left(\frac{m}{2kT}\right)^{3/2}\left(\frac{M}{2kT}\right)^{3/2} \times \int\int\int\int e^{-\frac{m+M}{2kT}W^2} e^{-\frac{\mu}{2kT}g^2} w g_1(1 - \cos(\chi)) g b db d\epsilon dW_i dg_i \tag{B.31}$$

Knowing that $wg_1 = z_1 g_1 = \left(W_1 + \frac{m}{m+M}g_1\right)g_1$, one can integrate over the centre of mass velocity and over all ϵ angles:

$$a_{00}(1) = 2\frac{\mu}{2kT}\left(\frac{\mu}{2\pi kT}\right)^{3/2}\frac{m}{m+M}\int\int e^{-\frac{\mu}{2kT}g^2} g_1^2 g 2\pi(1 - \cos(\chi)) b db dg_i \tag{B.32}$$

Changing the relative velocity coordinates to spherical with $g_j = g(\cos\theta_g, \sin\theta_g\cos\phi_g, \sin\theta_g\sin\phi_g)$ with $g_1 = g\cos\theta_g$ and $dg_i = g^2\sin\theta_g dg d\theta_g d\phi_g$ and integrating over the angles:

$$a_{00}(1) = \frac{8\pi}{3}\frac{\mu}{2kT}\left(\frac{\mu}{2\pi kT}\right)^{3/2}\frac{m}{m+M}\int\int e^{-\frac{\mu}{2kT}g^2} g^5 2\pi(1 - \cos(\chi)) b db dg \tag{B.33}$$

Making g dimensionless through the use of the velocity $h_g = \mu/2kT$, expression B.33 becomes:

$$a_{00}(1) = \frac{8}{3}\sqrt{\frac{2kT}{\pi\mu}}\frac{m}{m+M}\int\int e^{-g^{*2}} g^{*5} 2\pi(1 - \cos(\chi)) b db dg^* \tag{B.34}$$

To simplify the picture, one can introduce the definition of collision integrals which cannot be integrated until the deflection angle (or more specifically, the potential interaction) is specified. There are several equivalent ways of defining collision integrals, whereas here we present two very common ones:

$$\Omega^{(l)}(n) = \sqrt{\frac{kT}{2\pi\mu}}\int e^{-g^{*2}} g^{*2n+3} Q^{(l)} dg^* \tag{B.35}$$

$$\Omega(l,n) = \int e^{-g^{*2}} g^{*2n+3} Q^{(l)} dg^* \tag{B.36}$$

$$Q^{(l)} = \int 2\pi(1 - cos^l(\chi)) b db \tag{B.37}$$

The collision integral in Equation (B.35) has units of volumetric flux while only of area in Equation (B.36). Given these definitions, $a_{00}(1)$ becomes:

$$a_{00}(1) = \frac{16}{3}\frac{m}{m+M}\Omega^{(1)}(1) \tag{B.38}$$

And a first approximation for mobility:

$$\langle K\rangle_I = \frac{3}{16}\frac{e}{n}\sqrt{\frac{2\pi}{\mu kT}}\frac{1}{\Omega(1,1)} \tag{B.39}$$

It suffices to say that this expression and that of Appendix A (Equation (A.39)) or that of Mason and Schamp are equivalent with the only difference that the ion in this case is considered spherical. If the ion were not spherical, as is normally the case, one can assume that all orientations are equally probable in which case, the collision integral can now be averaged over all orientation angles (θ, ϕ, γ):

$$\Omega(1,1)_{Av} = \bar{\Omega}(1,1) = \Omega_{1,1} = \frac{1}{8\pi^2}\int_0^{2\pi}\int_0^{\pi}\sin\phi\int_0^{2\pi}\int e^{-g^{*2}} g^{*5} Q^{(l)} dg^* d\theta d\phi d\gamma \tag{B.40}$$

When compared to how the expression on Appendix A was obtained, one could initially consider that since the Chapman-Enskog linearisation ($v_d \ll kT/m$) yields a solution where the mobility is independent of the field (in a similar fashion to the 1st approximation here), it would seem plausible that allowing more terms of the Chapman-Enskog expansion (in Equation (A.27)) would yield an expression dependent on the field. However, in Appendix A, specifically Equation (A.2), a symmetric ion velocity distribution was assumed so the question arises whether the symmetric ion distribution is also correct at higher fields. As will be seen later, the assumed distribution does not hold for high fields so the validity of any results for non-vanishing drift velocities using a presumed ion distribution may be questioned at this point.

One would like to generalise the results of the moment calculations by calculating yet another $a_{rs}(l)$ for the sake of completion, $a_{11}(0)$. $a_{11}(0)$ is equivalent to calculating the ion's energy at vanishing fields. When trying to calculate the value of $\langle\psi_0^{(1)}\rangle_I = \langle\frac{3}{2} - \frac{Mz^2}{2kT}\rangle_I = \frac{3}{2} - \frac{M}{2kT}\langle z^2\rangle_I$ using Equation (B.18), one arrives at:

$$\frac{1}{2}a_{11}(0)\langle\psi_0^{(1)}\rangle_I = -\mathcal{E}[\langle\psi_1^{(0)}\rangle_I], \tag{B.41}$$

or

$$\langle z^2\rangle_I = \left(\frac{e}{Mn}\right)\frac{2\langle K\rangle_I E^2}{a_{11}(0)} - \frac{3kT}{M} = \left(\frac{eE}{Mn}\right)^2\frac{2}{a_{00}(1)a_{11}(0)} - \frac{3kT}{M}, \tag{B.42}$$

where only $a_{11}(0)$ is needed to obtain the ion's energy.

To calculate $a_{11}(0)$, $(\psi_0^{(1)}, \psi_0^{(1)}) = 3/2$. Therefore:

$$a_{11}(0) = \frac{2}{3}(\psi_0^{(1)}, \mathcal{J}\psi_0^{(1)}) = \frac{2}{3}\int\int\int\int fF^{(0)}\left(\frac{3}{2} - \frac{Mz^2}{2kT}\right)\frac{M}{2kT}(z'^2 - z^2)gbdbd\epsilon dz_i dc_i \tag{B.43}$$

Considering that:

$$z^2 - z'^2 = \tilde{z}^2 - \tilde{z}'^2 + 2W_j(z_j - z_j') = 2W_j(z_j - z_j'); \text{since } \tilde{z} = \tilde{z}', \tag{B.44}$$

then Equation (B.43) becomes after integrating over ϵ:

$$a_{11}(0) = \frac{2}{3}\int\int\int F^{(0)} f\left(\frac{3}{2} - \frac{Mz^2}{2kT}\right)\frac{M}{2kT}2W_j(z_j - z_j')g2\pi\, bdbdz_i dc_i \tag{B.45}$$

Translating variables to relative velocity and centre of mass velocity as per usual, one arrives at:

$$a_{11}(0) = -\frac{2\pi}{3}\left(\frac{m}{2\pi kT}\right)^{3/2}\left(\frac{M}{2\pi kT}\right)^{5/2}\frac{m}{m+M}\int\int e^{-\frac{m+M}{2kT}W^2}e^{-\frac{\mu}{2kT}g^2}$$
$$\times\left(\frac{3}{2} - \frac{M}{2kT}\left(W^2 + \left(\frac{m}{m+M}\right)^2 g^2 + \frac{2m}{m+M}W_j g_j\right)\right)2W_j g_j g Q^{(l)} dW_i dg_i \tag{B.46}$$

Which, if integrated over the centre of mass velocity becomes:

$$a_{11}(0) = \frac{8\pi^2}{3}\left(\frac{m}{2\pi kT}\right)^{\frac{3}{2}}\left(\frac{M}{2\pi kT}\right)^{\frac{7}{2}}\left(\frac{m}{m+M}\right)^2 \int e^{-\frac{\mu}{2kT}g^2}\left(\frac{\pi^{3/2}}{2\left(\frac{m+M}{2kT}\right)^{5/2}}\right) g^3 Q^{(l)} dg_i \tag{B47}$$

Integrating over relative velocity angles and rearranging the equation:

$$a_{11}(0) = \frac{32}{3}\sqrt{\frac{kT}{2\pi\mu}}\frac{mM}{(m+M)^2}\int e^{-g^{*2}} g^{*5} Q^{(l)} dg_i^* = \frac{32}{3}\frac{mM}{(m+M)^2}\Omega^{(1)}(1) = \frac{2M}{m+M}a_{00}(1) \tag{B.48}$$

And the ion's energy therefore becomes:

$$\langle z^2\rangle_I = \left(\frac{eE}{Mn}\right)^2 \frac{2}{a_{00}(1)a_{11}(0)} - \frac{3kT}{M} = \left(\frac{eE}{Mn}\right)^2 \frac{(m+M)}{Ma_{00}(1)^2} - \frac{3kT}{M} = \frac{(m+M)}{M}\langle w\rangle_I^2 - \frac{3kT}{M} \tag{B.49}$$

Or, the total energy of the ion is given by

$$\frac{1}{2}M\langle z^2\rangle_I = \frac{3}{2}kT + \frac{1}{2}(m+M)\langle w\rangle_I^2 = \frac{3}{2}kT + \frac{1}{2}(m+M)\langle v_d\rangle_I^2 = \frac{3}{2}kT_b \tag{B.50}$$

Equation (B.50) is an expression known as Wannier's formula and has quite a strong repercussion. It specifies that the ion's energy is made up of the contribution of 3 very distinctive terms. The total energy of the ion is given by the thermal energy ($3/2kT$) plus the energy of the drift motion $1/2M\langle v_d\rangle_I^2$ directly from the field plus an extra energy term from the gas collisions due to this drift which increases the ion energy by $1/2m\langle v_d\rangle_I^2$. This also suggests that the ion may be perceived with a higher temperature than the gas and proportional to T_b, an effect that was the basis for the two-temperature theory. An interesting consequence of this result is that it may be used to prove that the ion distribution depicted in Appendix A is only valid under very particular scenarios. If one were to calculate the ion energy using Equation (A.2), the result would yield:

$$\frac{1}{2}M\langle z^2\rangle_{A2} = \frac{3}{2}kT + \frac{1}{2}M\langle v_d\rangle_{A2}^2 \tag{B.51}$$

Which when compared to Equation (B.50) is only true if $m \ll M$ (i.e. heavy ions in a light gas) and $\langle v_d\rangle_I^2 \ll kT/m$ (i.e. low fields). It is also valid for any ion under vanishing fields, $\langle v_d\rangle_I^2 \cong 0$ up to a correction, and hence applies as a first approximation for mobility as shown in Appendix A. Under all other scenarios, the distribution of Equation (A.2) will not yield a correct interpretation. One can also show that energy terms pertaining to velocities perpendicular to the direction of the field do not yield the correct ion energy when using Equation (A.2). For example, in the u direction, when sing Equation (A.2):

$$\frac{1}{2}M\langle u^2\rangle_{A2} - \frac{1}{2}kT = \frac{1}{2}M\frac{kT}{M} - \frac{1}{2}kT = 0 \tag{B.52}$$

which is the expected Maxwellian result. When the first approximation is used, however, the result yields (using Equations (B.22) and (B.23)):

$$\frac{1}{2}M\langle u^2\rangle_I - \frac{1}{2}kT = -\frac{1}{3}(\langle\psi_0^{(1)}\rangle_I + \langle\psi_2^{(0)}\rangle_I) = \frac{2\mathcal{E}^2}{3a_{00}(1)}\left(\frac{1}{a_{11}(0)} - \frac{1}{a_{00}(2)}\right) \tag{B.53}$$

And using the tables from Appendix B:

$$\frac{1}{2}M\langle u^2\rangle_I - \frac{1}{2}kT = \frac{2\mathcal{E}^2}{3a_{00}(1)a_{11}(0)a_{00}(2)}\left(\frac{16}{15}\frac{m}{(m+M)^2}(5M\Omega^{(1)}(1) + 3m\Omega^{(2)}(2)) - \frac{16}{3}\frac{mM}{(m+M)^2}\Omega^{(1)}(1)\right) = \frac{32\mathcal{E}^2}{15a_{00}(1)a_{11}(0)a_{00}(2)}\left(\frac{m^2}{(m+M)^2}\Omega^{(2)}(2)\right) \geq 0 \tag{B.54}$$

which is positive in general. It would only be 0 if $\frac{m}{m+M} = 0$ or if $M \gg m$ which is the same criterion as that for the distribution of Appendix A, and clearly shows that kinetic ion energy perpendicular to the ion movement is larger than expected from a Maxwellian distribution for any ion of non-infinite mass. In fact, if mobility is known, it should be possible to infer the mass from the ion's perpendicular energy.

As a final note, while it would seem that the results from Kihara's one-temperature theory may work for any field as long as a sufficient number of expansion terms is added, it turns out that the convergency of the series is very low. In particular, when compared to Lorentz model ($m \gg M$), it substantially deviates from exact results except for low to mid fields, hence the reason that Kihara's one-temperature theory is regarded as ion mobility for weak to mid-fields. A two-temperature theory (at least) is required for higher convergence.

Appendix C. Derivation of the two-temperature theory

A big problem dealing with the one-temperature theory is its weak convergence at high fields. Even when the third approximation is employed, its result quickly diverges. The reason for its divergence is that the even powers of the field are directly proportional to E/n, which increases without bound as the electric field increases. For example, the term $\alpha_2(E/n)^2$ would require and additional opposite sign term of higher order to correct the upset $\alpha_3(E/n)^4$. However, as the field increases further, this term would very quickly require a new higher-order term to correct its imbalance and so on. From a more careful look, the expansion terms are however not exactly proportional to E/n, but to $(\mathcal{E}/(a_{00}(1)))^2$, which suggests a denominator proportional to temperature of the type $T\Omega(1,1)$. While this denominator would remain fixed as the field increases, a small change suggesting a dependence on a temperature that increases with the field (for example the ion temperature T_b suggested from Wannier's formula) may lead to cancelling the unbound increase of the field. The main concept therefore for the two-temperature approximation is to set the ion temperature to a different temperature than that of the gas molecules. The idea is that the ion temperature T_b is set to be close to the mean ion energy, e.g. $\frac{3}{2}kT_b = \frac{1}{2}M\langle z^2\rangle$. While other similar temperature choices can be chosen for T_b, there are advantages to using this result. The inclusion of two temperatures brings more difficulty than could have been expected at first as it makes the $\mathcal{J}$ operator no-longer symmetric. This turned out not to be an unsurmountable problem, but it was one that held back the theory of ion-mobility for over 20 years.

To calculate the collision integral quadratures, there is no requirement to know the exact value T_b, but its value is needed in order to fully integrate the quadrature. Since T_b depends on the drift velocity, this choice will couple the equations of drift and energy. To start, we may modify the ion distribution at equilibrium using T_b which becomes:

$$F^{(0)} = \left(\frac{M}{2\pi kT_b}\right)^{\frac{3}{2}} e^{-\frac{M(z_i)^2}{2kT_b}} \tag{C.1}$$

The process of calculating the moments of the equation are quite similar to those that have been followed for the one-temperature theory. However, one must be careful mainly due to two reasons. The first is that the $a^*_{rs}(l)$ coefficients, even though the definition remains the same as that of Equation (B.13), the calculations are different due to the involvement of T_b in Equation (C.1). As such we have added the $*$ to differentiate the coefficients from those of the one-temperature theory. The second, which is a consequence of the non-symmetry, is that not all off-diagonal terms are zero even for the case of the Maxwell model ($4-\infty$). It can be shown that the off-diagonal terms $a_{rs}(l)$ values for the Maxwell model however vanish for $s > r$. This will add some new terms to the previously calculated approximations for the one-temperature theory. For example, using Equation (B.22) instead of (B.18) for the first approximation, with the criteria that summation terms for $s > r$ vanish yields:

$$\langle \psi_0^{(1)}\rangle_I = -\frac{2\mathcal{E}}{a^*_{11}(0)}\langle \psi_1^{(0)}\rangle_I - \frac{a^*_{10}(0)}{a^*_{11}(0)} = -\frac{2\mathcal{E}^2}{a^*_{11}(0)a^*_{00}(1)} - \frac{a^*_{10}(0)}{a^*_{11}(0)} \tag{C.2}$$

Table B.1. Common eigenfunctions and eigenvalues of the Maxwell model (special case with independence of the collision integral on the velocity).

l, r	$\psi_l^{(r)}$	$\left(\frac{\pi\mu}{2kT}\right)^{1/2}\lambda_l^{(r)}$
0,0	1	0
1,0	w	$\frac{8}{3}\frac{m}{m+M}\bar{\Omega}(1,1)$
0,1	$\frac{3}{2}-z^2$	$\frac{16}{3}\frac{mM}{(m+M)^2}\bar{\Omega}(1,1)$
1,1	$w\left(\frac{5}{2}-z^2\right)$	$\frac{8}{15}\frac{m}{(m+M)^3}[5(3M^2+m^2)\bar{\Omega}(1,1)+8mM\bar{\Omega}(2,2)]$
2,0	$\frac{1}{2}(3w^2-z^2)$	$\frac{16}{15}\frac{m}{(m+M)^2}[5M\bar{\Omega}(1,1)+3m\bar{\Omega}(2,2)]$
0,2	$\frac{1}{2}\left(\frac{15}{4}-5w^2+w^4\right)$	$\frac{32}{15}\frac{mM}{(m+M)^4}[5(M^2+m^2)\bar{\Omega}(1,1)+4mM\bar{\Omega}(2,2)]$
2,1	$\frac{1}{2}(3w^2-z^2)\left(\frac{7}{2}-z^2\right)$	$\frac{16}{105}\frac{m}{(m+M)^4}\left[\frac{35}{2}M(4M^2+m^2)\bar{\Omega}(1,1)+7m(11M^2+3m^2)\bar{\Omega}(2,2)+72m^2M\bar{\Omega}(3,3)\right]$
1,2	$\frac{1}{2}w\left(\frac{35}{4}-7z^2+z^4\right)$	$\frac{128}{105}\frac{m}{(m+M)^5}\left[\frac{35}{16}(5M^4+6m^2M^2+m^4)\bar{\Omega}(1,1)+7mM(2M^2+m^2)\bar{\Omega}(2,2)+12m^2M^2\bar{\Omega}(3,3)\right]$
2,2	$\frac{1}{4}(3w^2-z^2)\left(\frac{63}{4}-9z^2+z^4\right)$	$\frac{16}{35}\frac{m}{(m+M)^6}\left[35M^3(M^2+m^2)\bar{\Omega}(1,1)+7m(3M^2+m^2)^2\bar{\Omega}(2,2)+16m^2M(7M^2+3m^2)\bar{\Omega}(3,3)+\frac{512}{9}m^3M^2\bar{\Omega}(4,4)\right]$

Table B.2. $a_{rs}(l)$ expansion coefficients for Kihara's first temperature theory.

r,s	l	$\left(\frac{\pi\mu}{2kT}\right)^{\frac{1}{2}} a_{rs}(l)$
$0,s$	0	0
1,1		$\frac{16}{3}\frac{mM}{(m+M)^2}\bar{\Omega}(1,1)$
1,2		$\frac{32}{15}\frac{m^2M}{(m+M)^3}[5\bar{\Omega}(1,1)-6\bar{\Omega}(1,2)]$
2,2		$\frac{16}{15}\frac{mM}{(m+M)^4}[5(2M^2+5m^2)\bar{\Omega}(1,1)-60m^2\bar{\Omega}(1,2)+48m^2\bar{\Omega}(1,3)+8mM\bar{\Omega}(2,2)]$
0,0	1	$\frac{8}{3}\frac{m}{m+M}\bar{\Omega}(1,1)$
0,1		$\frac{8}{15}\left(\frac{m}{m+M}\right)^2[5\bar{\Omega}(1,1)-6\bar{\Omega}(1,2)]$
0,2		$\frac{8}{105}\left(\frac{m}{m+M}\right)^3[35\bar{\Omega}(1,1)-84\bar{\Omega}(1,2)+48\bar{\Omega}(1,3)]$
$0,s$		$(-1)^s\frac{2\pi^{1/2}}{\Gamma\left(s+\frac{5}{2}\right)}\left(\frac{m}{m+M}\right)^{s+1}T^{s-1/2}\frac{d^2}{dT^s}[T^{1/2}\bar{\Omega}(1,1)]$
1,1		$\frac{4}{15}\frac{m}{(m+M)^3}[5(6M^2+5m^2)\bar{\Omega}(1,1)-60m^2\bar{\Omega}(1,2)+48m^2\bar{\Omega}(1,3)+16mM\bar{\Omega}(2,2)]$
1,2		$\frac{128}{105}\frac{m^2}{(m+M)^4}\left[\frac{35}{32}(12M^2+5m^2)\bar{\Omega}(1,1)-\frac{63}{16}(4M^2+5m^2)\bar{\Omega}(1,2)+\frac{57}{2}m^2\bar{\Omega}(1,3)-15m^2\bar{\Omega}(1,4)+7mM\bar{\Omega}(2,2)-8mM\bar{\Omega}(2,3)\right]$
2,2		$\frac{128}{105}\frac{m}{(m+M)^5}\left[\frac{35}{128}(40M^4+168m^2M^2+35m^4)\bar{\Omega}(1,1)-\frac{21}{16}m^2(84M^2+35m^2)\bar{\Omega}(1,2)+\frac{3}{4}m^2(108M^2+133m^2)\bar{\Omega}(1,3)-105m^4\bar{\Omega}(1,4)+45m^4\bar{\Omega}(1,5)+\frac{7}{2}mM(4M^2+7m^2)\bar{\Omega}(2,2)-56m^3M\bar{\Omega}(2,3)+40Mm^3\bar{\Omega}(2,4)+12m^2M^2\bar{\Omega}(3,3)\right]$

0, 0	2	$\frac{16}{15}\frac{m}{(m+M)^2}[5M\bar{\Omega}(1,1)+3m\bar{\Omega}(2,2)]$
0, 1		$\frac{16}{15}\frac{m^2}{(m+M)^3}\left[5M\bar{\Omega}(1,1)-6M\bar{\Omega}(1,2)+3m\bar{\Omega}(2,2)-\frac{24}{7}m\bar{\Omega}(2,3)\right]$
0, 2		$\frac{16}{15}\frac{m^3}{(m+M)^4}\left[5M\bar{\Omega}(1,1)-12M\bar{\Omega}(1,2)+\frac{48}{7}M\bar{\Omega}(1,3)+3m\bar{\Omega}(2,2)-\frac{48}{7}m\bar{\Omega}(2,3)+\frac{80}{21}m\bar{\Omega}(2,4)\right]$
1, 1		$\frac{128}{105}\frac{m}{(m+M)^4}\left[\frac{35}{16}M(4M^2+7m^2)\bar{\Omega}(1,1)-\frac{147}{4}m^2M\bar{\Omega}(1,2)+24m^2M\bar{\Omega}(1,3)+\frac{7}{16}m(22M^2+21m^2)\bar{\Omega}(2,2)-21m^3\bar{\Omega}(2,3)+15m^3\bar{\Omega}(2,4)+9m^2M\bar{\Omega}(3,3)\right]$
		$a_{sr}(l)=a_{rs}(l)\frac{r!\Gamma\left(l+s+\frac{3}{2}\right)}{s!\Gamma\left(l+r+\frac{3}{2}\right)};\bar{\Omega}(l,s+1)=\bar{\Omega}(l,s)+\frac{T}{s+2}\frac{d\bar{\Omega}(l,s)}{dT}$

$\mathcal{E} = \left(\frac{eE}{Mn}\right)\left(\frac{M}{2kT_b}\right)^{1/2}$ slightly modified from Appendix B. Equation (C.2) differs from Equation (B.22) due to off diagonal terms. In all, however, the approximations for mobility are similar to those of Appendix B with minor modifications. For the first two approximations, one gets:

$$\langle K_{2T}\rangle_I = \frac{e}{Mn}\frac{1}{a^*_{00}(1)} \tag{C.3}$$

$$\langle K_{2T}\rangle_{II} = \langle K_{2T}\rangle_I \left[1 + \frac{a^*_{01}(1)}{a^*_{11}(1)}\left\{\frac{a^*_{10}(1)}{a^*_{00}(1)} + \frac{5}{3}\frac{a^*_{10}(0)}{a^*_{11}(0)}\right\} + \left(\frac{\mathcal{E}}{a^*_{00}(1)}\right)^2 \frac{2}{3}\frac{a^*_{01}(1)}{a^*_{11}(1)}\left[\frac{5a^*_{00}(1)}{a^*_{11}(0)} + \frac{4a^*_{00}(1)}{a^*_{00}(2)}\right]\right] \tag{C.4}$$

Where the first approximation is equivalent to the one-temperature theory except for the need to re-calculate $a^*_{00}(1)$ and the second one only has one additional term when compared to Kihara's one-temperature theory. What's more important, both approximations C.3 and C.4 are within 10% of the full numerical calculation for the whole range of fields when compared to the Lorentz model ($m \gg M$) which fairs significantly better than the result from Kihara and makes the two-temperature theory a much better recourse for high fields. To better understand the reason behind it, one must first calculate some of the $a^*_{rs}(l)$. For example, one can start with $a^*_{00}(1)$. To do so, we follow a similar approach to what has been done previously:

$$a^*_{00}(1) = 2(\psi^{(0)}_1, \mathcal{J}\psi^{(0)}_1) = 2\frac{M}{2kT_b}\int\int\int\int F^{(0)} f w(w - w')gbdbd\epsilon dz_i dc_i \tag{C.5}$$

Using typical relations for relative velocity and centre of mass velocity and:

$$F^{(0)}f = \pi^{-3}\left(\frac{m}{2kT}\right)^{3/2}\left(\frac{M}{2kT_b}\right)^{3/2} e^{-B}$$

$$B = \left(\frac{m}{2kT} + \frac{M}{2kT_b}\right)W^2 + \frac{2mM}{m+M}\left(\frac{1}{2kT_b} - \frac{1}{2kT}\right)W_i g_i + \frac{mM}{(m+M)^2}\left(\frac{M}{2kT} + \frac{m}{2kT_b}\right)g^2$$

$$e_\mu = \frac{m}{m+M}\,;\; d = \frac{mT_b}{MT + mT_b}\,;\; f = e_\mu d\frac{M(T_b - T)}{mT_b} \tag{C.6-10}$$

one arrives at:

$$a^*_{00}(1) = 2\pi^{-3}\frac{Me_\mu}{2kT_b}\left(\frac{m}{2kT}\right)^{3/2}\left(\frac{M}{2kT_b}\right)^{3/2} \times \int\int\int\int e^{-B}(W_1 + e_\mu g_1)g_1 g(1 - \cos(\chi))bdbd\epsilon dW_i dg_i \tag{C.11}$$

To simplify calculations before we integrate the centre of mass velocity, one can do a change of variables so that the exponential becomes a quadratic function:

$$W'_i = W_i - fg_i; dW_i dg_i = dW'_i dg_i; B = e^{-\frac{mW'^2}{2dkT} - \frac{\mu g^2}{2kT_{eff}}}$$

where $T_{eff} = \frac{MT+mT_b}{M+m}$ is an effective temperature of the gas-ion pair that will become crucial to the determination of the collision integrals. Introducing the new change of variable in C.11 and integrating over the new centre of mass velocity:

$$a^*_{00}(1) = 2e_\mu\pi\left(\frac{Md}{2\pi kT_b}\right)^{5/2}\int\int\int e^{-\frac{\mu g^2}{2kT_{eff}}} g_1^2 g(1 - \cos(\chi))bdbd\epsilon dg_i \tag{C.12}$$

Integrating over relative velocity angles and using the relation $\frac{Md}{T_b} = \frac{\mu}{T_{eff}}$ one arrives at:

$$a^*_{00}(1) = \frac{8}{3}e_\mu\left(\frac{2kT_{eff}}{\pi\mu}\right)^{1/2}\int\int\int e^{-g^{*2}} g^{*5} Q^{*(l)} dg^* = \frac{16}{3}e_\mu\left(\frac{kT_{eff}}{2\pi\mu}\right)^{\frac{1}{2}}\Omega^*(1,1) \tag{C.13}$$

where the * on $\Omega^*(1,1)$ is to specify that its calculation depends on the effective temperature T_{eff} and not on the temperature of the gas T. The expression $\Omega_{T_{eff}}(1,1)$, as well as $\Omega_T(1,1)$, may also be used with the same purpose. The first approximation to the mobility finally becomes:

$$\langle K_{2T}\rangle_I = \frac{3}{16}\frac{e}{n}\left(\frac{2\pi}{\mu k T_{eff}}\right)^{\frac{1}{2}}\frac{1}{\Omega^*(1,1)} \tag{C.14}$$

Other $a^*_{rs}(l)$ can be inferred in a similar manner and have been provided in Table C.I.

The effective temperature proposed here has a very clear physical meaning. Given that the mean relative energy of collision is given by

$$\langle E\rangle = \frac{1}{2}\mu\langle g^2\rangle = \frac{1}{2}\mu\langle (c_i - z_i)^2\rangle = \frac{1}{2}\mu(\langle c^2\rangle + \langle z^2\rangle),$$

and using the knowledge that $\frac{1}{2}m\langle c^2\rangle = 3/2kT$ and the definition of T_b, one arrives at:

$$\langle E\rangle = \frac{\mu}{m}\frac{3}{2}kT + \frac{\mu}{M}\frac{3}{2}kT_b = \frac{3}{2}k\frac{mT_b + MT}{m+M} = \frac{3}{2}kT_{eff} \tag{C.15}$$

so that the mean relative energy of collision is described by the effective temperature. Another interesting feature of T_{eff} is that for cases where $M \gg m$, e.g. large particles, the effect of the ion temperature is much smaller and Kihara's one-temperature approximation becomes accurate and so does Equation (A.2) for the distribution. On the other hand, one could probe Equation (A.2) with T_{eff} as the distribution temperature instead of T. In that case, Equation (A.2) would become:

$$F(z_i) = \left(\frac{M}{2\pi k T_{eff}}\right)^{3/2} e^{-\frac{M(z_i - v_{di})^2}{2kT_{eff}}} \tag{C.16}$$

Interestingly enough, the ion's energy when using the above distribution yields:

$$\frac{1}{2}M\langle z^2\rangle_{C16} = \frac{3}{2}kT_{eff} + \frac{1}{2}M\langle v_d\rangle^2_{C16} = \frac{3}{2}kT + \frac{1}{2}m\langle v_d\rangle^2_{C16} + \frac{1}{2}M\langle v_d\rangle^2_{C16} = \frac{3}{2}kT_b \tag{C.17}$$

which is equivalent to the ion's energy from Wannier's formula. The new distribution is therefore valid and a reasonable approximation for any ion mass and field (does not require in principle that $v_d \ll (kT/m)^{1/2}$). More importantly, it shows that T_{eff} represents the thermal energy ($3kT/2$) and the collisional energy ($1/2m\langle v_d\rangle^2$) which together with the field energy ($1/2M\langle v_d\rangle^2$), represent the ion's temperature T_b. Here the only term that is not exactly known is that related to the collisional energy portion. The reason why the ion distribution C.16 works and not for example if one were to use T_b instead of T_{eff} relies on the fact that for the gas-ion relative interaction, which establishes the mobility, the relative energy is given indeed by T_{eff} and the additional field term $1/2M\langle v_d\rangle^2$ does not affect this interaction directly.

Despite this great outcome, it is reasonable, and expected, to incorporate higher-order approximations to our result. In fact, our result would be exact – within the free molecule flight – if we were to find the exact expression for the collisional energy term. What is the exact value of T_{eff}? Will the distribution remain symmetric for all fields? Until these questions are answered, one must content himself with calculating approximations. This process, contrary to what happened with the one-temperature theory, is convoluted as higher approximations do not only affect the mobility K but the ion energy as well. If one were to add higher-order terms to the mobility approximation, it would be unwise not to add them to the ion's energy calculation, which would in turn affect the result of T_b and hence of T_{eff} and indirectly on the mobility. The second mobility approximation can be defined (after some work) as

$$\langle K_{2T}\rangle_{II} = \frac{3}{16}\frac{e}{n}\left(\frac{2\pi}{\mu k T_{eff}}\right)^{\frac{1}{2}}\frac{1+\alpha^*}{\Omega^*(1,1)} \tag{C.18}$$

with

$$\frac{3}{2}kT_{eff} = \frac{3}{2}kT + \frac{1}{2}m\langle v_d\rangle_I^2(1+\beta^*) \tag{C.19}$$

Table C.1. $a^*_{rs}(l)$ expansion coefficients for the two-temperature theory. (Note the non-symmetry of the terms).

r,s	l	$\frac{\left(\frac{\pi\mu}{2kT_{eff}}\right)^{\frac{1}{2}} a^*_{rs}(l)}{e_\mu \bar{\Omega}^*(1,1)}$
$0,s$	0	0
$1,0$		$-8\frac{f}{d}$
$1,1$		$\frac{8}{3}[2(1-e_\mu)+f(6C^*-5)]$
$1,2$		$-\frac{8d}{15}[4(1-d)(6C^*-5)-3f(4B^*-5)]$
$2,0$		$-\frac{4}{d^2}[10e_\mu f^2-f({e_\mu}^2+f^2)(6C^*-5)-3f(4B^*-5)]$
$2,1$		$-\frac{4}{3d}[10f(1-4e_\mu+4{e_\mu}^2)+2(6C^*-5)\{d^2(1-d)-fd(2-3d+11f)+f^2(4+7f)\}-3f(4B^*-5)({e_\mu}^2+f^2)+4e_\mu A^*\{4f(1-e_\mu)+f^2d(8E^*-7)\}]$
$2,2$		$\frac{4}{15}[40(1-e_\mu)(1-2e_\mu-2{e_\mu}^2)+2(6C^*-5)\{d^2(1-d)-fd(2-3d+11f)+f^2(4+7f)\}+3(4B^*-5)\{5f(d^2+2{e_\mu}^2+2f^2)-4(1-d)({e_\mu}^2+3f^2)\}$ $+15f({e_\mu}^2+f^2)(32D^*-21)+32(1-e_\mu)^2e_\mu A^*+8efA^*(8E^*-7)\{4(1-d)-5f\}+4e_\mu f^2A^*(80G^*-63)]$
$0,0$	1	$\frac{8}{3}$
$0,1$		$-\frac{8d}{15}(6C^*-5)$
$0,2$		$-\frac{8d^2}{21}[4(6C^*-5)+3(4B^*-5)]$
$1,0$		$-\frac{4}{3d}[10f(1-2e_\mu)+(6C^*-5)({e_\mu}^2+3f^2)+8e_\mu fA^*]$
$1,1$		$\frac{4}{15}[10(3-6e_\mu+4{e_\mu}^2)+(6C^*-5)\{5({e_\mu}^2+3f^2)-5d^2+22f(1-d)\}-3(4B^*-5)({e_\mu}^2+3f^2)+4e_\mu A^*\{4(1-e_\mu)+2f(8E^*-7)\}]$
$0,0$	2	$\frac{16}{15}[5(1-e_\mu)+f(6C^*-5)+3e_\mu A^*]$
$0,1$		$\frac{16d}{105}[(6C^*-5)\{7(d-1)-3f\}+3f(4B^*-5)-3e_\mu A^*(8E^*-7)]$
		$A^*=\frac{\bar{\Omega}^*(2,2)}{\bar{\Omega}^*(1,1)}; B^*=5C^*-\frac{4\bar{\Omega}^*(1,3)}{\bar{\Omega}^*(1,1)}; C^*=\frac{\bar{\Omega}^*(1,2)}{\bar{\Omega}^*(1,1)}; D^*=\frac{\bar{\Omega}^*(1,4)}{\bar{\Omega}^*(1,1)}; E^*=\frac{\bar{\Omega}^*(2,3)}{\bar{\Omega}^*(2,2)}; F^*=\frac{\bar{\Omega}^*(3,3)}{\bar{\Omega}^*(1,1)}; G^*=\frac{\bar{\Omega}^*(2,4)}{\bar{\Omega}^*(2,2)}$

And where $(1+\alpha^*)$ corresponds to the expression in brackets of Equation (C.4) and $(1+\beta^*)$ is a correction to the collisional energy and comes from the calculation of the second approximation to the ion energy $\langle z^2\rangle_{II}$. This tedious calculation will yield (approximated):

$$\beta^* = \frac{M}{m}\left[2\frac{a^*_{01}(1)}{a^*_{11}(0)}\frac{\langle\psi_0^{(1)}\rangle_I}{\langle\psi_1^{(0)}\rangle_I} + \frac{a^*_{12}(0)}{a^*_{11}(0)}\frac{\langle\psi_0^{(2)}\rangle_I}{\langle\psi_1^{(0)2}\rangle_I}\right] \tag{C.20}$$

While better approximations may be obtained rather than Equation (C.18), our goal of showing possible weaknesses of the Mason-Schamp equation ends here with $\langle K_{2T}\rangle_{II}$ leaving the main text to foreshow some other simplifications that must be incorporated to study some effects not considered in any theoretical calculation.